

# Dust measurements with the Mars Dust Counter on board

## Nozomi (PLANET-B)

Harald Krüger, MPI für Sonnensystemforschung, Göttingen, Germany; Planetary Exploration Research Center, Chiba Institute of Technology, Narashino, Chiba, Japan,  
krueger@mps.mpg.de

Masanori Kobayashi, Planetary Exploration Research Center, Chiba Institute of Technology, Narashino, Chiba, Japan

Hiroshi Kimura, Planetary Exploration Research Center, Chiba Institute of Technology, Narashino, Chiba, Japan

Tomoko Arai, Planetary Exploration Research Center, Chiba Institute of Technology, Narashino, Chiba, Japan

Håkan Svedhem, Delft University of Technology, Delft, The Netherlands

Sho Sasaki, Graduate School of Science, Department of Earth and Space Science, Osaka University, Osaka, Japan

## Abstract

Nozomi was Japan's first space mission to Mars, launched on 3 July 1998 UT. It was equipped with the Mars Dust Counter (MDC) which was an impact ionisation dust detector. MDC detected 96 dust particle impacts when the spacecraft was in Earth orbit and later in interplanetary space, before its operation ended in April 2002 due to a technical failure on board. We compare the Nozomi dust measurements with the dust measurements obtained with the dust detector on board the Ulysses spacecraft. Impact speeds and masses of dust particles measured by Nozomi MDC are overall consistent with the measurements obtained by Ulysses in the same region of interplanetary space. Based on the impact speeds measured while Nozomi was in Earth orbit, MDC detected neither dust particles of natural origin that were bound to the Earth nor space debris. The dust impact rate measured in interplanetary space varied by approximately a factor of 2, consistent with theoretical predictions by the Interplanetary Meteoroid Engineering Model. The particle impact direction was concentrated towards the ecliptic plane, in agreement with an interplanetary origin of the majority of the measured dust particles. No impacts of cometary trail particles could positively be identified during known cometary trail crossings of Nozomi. The Nozomi dust data may become a valuable reference for the dust measurements to be obtained in the same region of interplanetary space with future space missions like, for example, MMX and DESTINY<sup>+</sup>.

## Keywords

## 1 Introduction

The Japanese spacecraft Nozomi, initially named PLANET-B, was launched on 3 July 1998 UT, heading towards Mars (Yamamoto and Tsuruda 1998). The mission's main scientific objective was the study of the structure and dynamics of the upper Martian atmosphere and its interaction with the solar wind (Nakatani et al. 1995). An additional objective was the search for a dust ring surrounding Mars (Ishimoto et al. 1997; Sasaki 1999) which had been predicted by several authors (e.g., Soter 1971; Hamilton 1996; Krivov and Hamilton 1997; Zakharov et al. 2014) but remains as yet undiscovered (Showalter et al. 2006;

Showalter 2017). More recent studies of the particle dynamics in the Martian rings were presented by Makuch et al. (2005); Krivov et al. (2006); Liu and Schmidt (2021). To this end, Nozomi was equipped with the Mars Dust Counter (MDC) which was an impact ionisation dust detector (Igenbergs et al. 1996, 1998), with strong heritage from earlier instruments (BREMSAT, Hiten, Galileo, Ulysses; Igenbergs et al. 1991; Iglseder et al. 1993; Grün et al. 1992a,b).

Although Nozomi could not fulfil its primary mission goals at Mars due to technical failures on board (see Section 2), the MDC measurements of cosmic dust in the vicinity of the Earth and the Moon and later in interplanetary space provided new scientific results. MDC detected 96 dust particles between 1998 and 2002. For 79 of them the impact speed and particle mass could be derived from the measured charge signals. Most of the detected particles were interplanetary dust orbiting the Sun but MDC also detected several particles of interstellar origin (Sasaki et al. 1999, 2002a,b, 2007; Senger 2007). Finally, an enhanced dust impact rate was recorded in November 1998 when the spacecraft – still being in Earth orbit – crossed the Leonids meteoroid stream.

The objectives of this paper are threefold. First, we want to make the Nozomi dust data set in electronic form available to the scientific community so that it can easily be accessed for further scientific investigations. To our knowledge, the Nozomi dust data are not electronically available so far. Similarly, 20 years of dust measurements collected with the DEBris In orbit Evaluator 1 (DEBIE-1) dust impact detector on board the Project for On-Board Autonomy (PROBA-1) mission in Low Earth orbit was also recently reanalysed and became available to the scientific community (Azzi et al. 2025). Second, new modelling tools for the dynamics of interplanetary dust have become available since the MDC data were collected about 25 years ago, and we want to compare the predictions of those models with the MDC measurements. Finally, we review the Nozomi dust measurements in view of the upcoming Martian Moons eXploration (MMX) and Demonstration and Experiment of Space Technology for INterplanetary voYage Phaethon fLyby and dUst Science (DESTINY<sup>+</sup>) space missions, to be launched in 2026 and 2028, respectively (Kuramoto et al. 2022; Ozaki et al. 2022; Arai and Destiny<sup>+</sup> Team 2024). We expect that the Nozomi data will become a valuable reference for both upcoming space missions, given that both of them will be equipped with in situ dust instruments and traverse the same regions of space between Earth and Mars as Nozomi did.

In Section 2 we give a brief overview of the Nozomi mission, and in Section 3 we describe the Mars Dust Counter (MDC) on board the spacecraft. Section 4 gives an overview of the Nozomi dust data set and

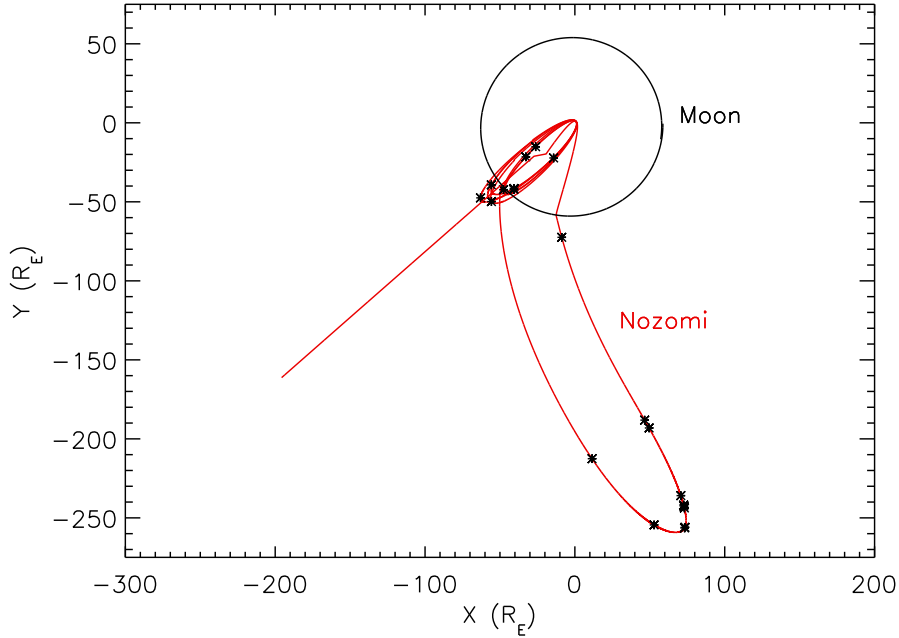


Figure 1. : Nozomi trajectory when the spacecraft was in Earth orbit between launch on 3 July 1998 and 25 December 1998 (red), projected onto the ecliptic plane (vernal equinox is to the right). The orbit of the Moon is shown in black, and the measured dust impacts are superimposed (asterisks). The units are mean Earth radii ( $R_E = 6,371$  km). The Nozomi trajectory data were provided by ISAS/JAXA.

in Section 5 we present a new comprehensive analysis of the Nozomi dust data. Section 6 is a discussion, and in Section 7 we summarise our conclusions.

## 2 Nozomi Mission

On 3 July 1998 UT, the PLANET-B spacecraft was launched at Kagoshima Space Center and renamed to Nozomi, following a Japanese tradition. The spacecraft was initially brought onto a highly elliptical geocentric trajectory with apogee beyond the lunar orbit (Kawaguchi et al. 1995). As the available energy provided by the launcher was not sufficient for a direct injection into a Mars transfer orbit, a few gravitational manoeuvres were necessary. The first swing-by at the Moon took place on 24 September 1998, and brought Nozomi to an apogee distance of 1.7 million kilometres from Earth (Figure 1). After a second lunar swing-by, a powered Earth swing-by on 20 December 1998 was supposed to bring Nozomi onto its final Mars transfer trajectory. Due to a problem in the propulsion system during the Earth swing-by, however, the spacecraft did not receive enough energy to reach Mars on a direct trajectory.

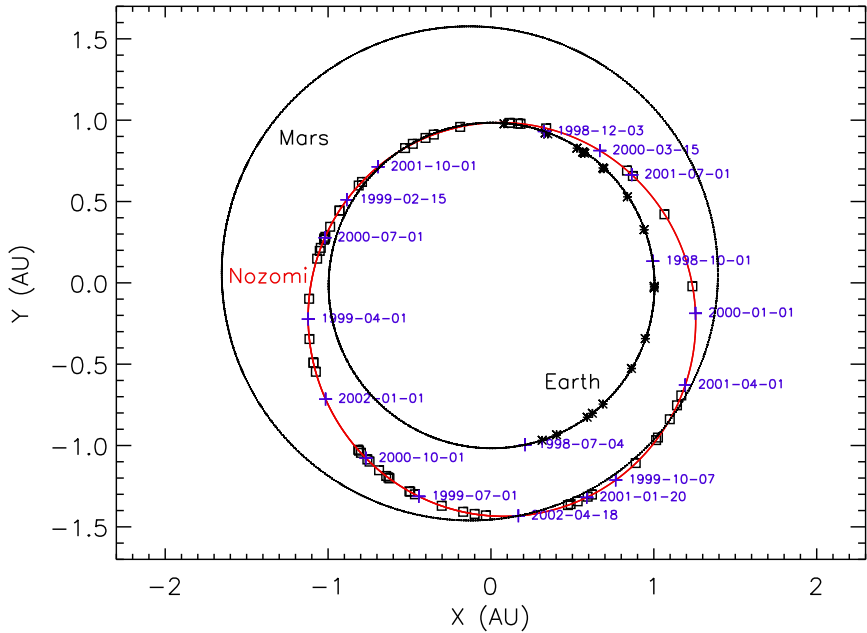


Figure 2. : Nozomi trajectory projected onto the ecliptic plane (vernal equinox is to the right). The interplanetary trajectory of the spacecraft is shown in red. The measured particle impacts are superimposed for the Earth orbiting phase (asterisks) and for the interplanetary trajectory (squares). The locations of the spacecraft at specific times are indicated in blue. The Nozomi trajectory data were provided by ISAS/JAXA.

Thus, Nozomi's interplanetary trajectory had to be changed completely (Yoshikawa et al. 2005), and the injection into Mars orbit – originally planned for October 1999 – had to be postponed to December 2003.

The interplanetary trajectory of the spacecraft is shown in Figure 2. During the interplanetary mission phase the Nozomi orbital plane was close to the ecliptic plane within a few degrees.

Unfortunately, the mission suffered from additional technical problems. Particularly severe was the damage of a power supply unit which occurred on 24 April 2002. It was probably caused by a solar eruption which had occurred a few days earlier (Forbes et al. 2005) and hit the spacecraft. As a consequence, Nozomi could not enter Mars orbit and passed by the red planet on 12 December 2003 at an altitude of 894 km. Finally, the mission was declared lost on 10 January 2004 after the exact spacecraft position could not be determined, and a telemetry link could not be established anymore. Nevertheless, Nozomi provided valuable in situ dust measurements in the interplanetary space between Earth and Mars.

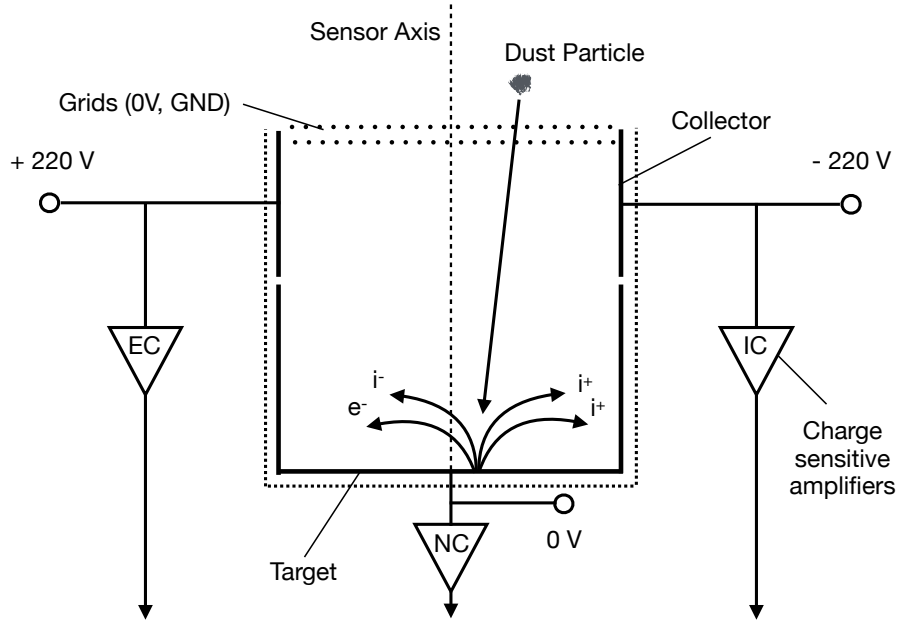


Figure 3. : Measurement principle of MDC. Impacting dust particles vaporised when hitting the target and produced plasma around the impact location. The charges of this plasma (negative free electrons and positive ions) were separated by the electric field inside the sensor box. Positive ions were collected by the negatively biased ion channel collector and electrons were collected by the positively biased electron channel collector. Three charge sensitive logarithmic amplifiers converted the measured charges into voltage signals that were transformed into digital data and transmitted to Earth.

### 3 Mars Dust Counter (MDC) Overview and Operation

#### 3.1 Instrument Overview

The Mars Dust Counter (MDC) was a light-weight impact ionisation dust detector developed mainly by the Technical University of Munich in Germany, and the European Space Research and Technology Centre of the European Space Agency (ESA-ESTEC; Igenbergs et al. 1996, 1998). It was an improved version of the dust detectors flown on board the BREMSAT and Hiten (MUSES-A) spacecraft which measured dust particles in low Earth orbit and in the Earth-Moon region, respectively (Igenbergs et al. 1991; Iglseder et al. 1993; Münzenmayer et al. 1997). The MDC was designed to determine not only the flux but also the mass and speed of impacting dust particles by measuring the ion and the electron charges produced by high speed impacts onto gold plate targets (impact speed  $v_{\text{imp}} > 1\text{ km s}^{-1}$ ). In addition, the

particle impact direction could be determined from the sensor orientation during the impact.

A sketch of the MDC is shown in Figure 3. Dust particles vaporise upon impact when they hit the target and produce a plasma cloud. The charges of this plasma are separated by the electric field inside the sensor box. Positive ions are collected by the ion collector, and electrons are collected by the electron collector. Up to three charge signals are measured for each impact. Charge sensitive amplifiers convert the charges into voltage signals that are further transformed into digital data and transmitted to Earth. From the measured charge signals and the delay times the location of the impact onto the sensor can be determined and subsequently used to constrain the impact trajectory of the particle. Finally, the impact speed and mass of the particle are derived from the charge signal's rise time, the charge amplitude and the impact position on the sensor box. The uncertainty of the impact speed is a factor of 2 and that of the mass determination is a factor of 5, respectively (Naumann 2000).

Entrance grids shield the instrument from the ambient space plasma to reduce noise signals. For impact angles up to  $80^\circ$  w.r.t. the sensor axis, i.e. w.r.t. the vertical direction in Figure 3, the penetrability of the grids for particles in the size range between  $0.1\text{ }\mu\text{m}$  and  $10\text{ }\mu\text{m}$  is nearly constant at about 92% to 95% (Senger 2007).

The mass of MDC was only 730 g and, thus, much lower than that of comparable impact ionisation dust detectors on board the Galileo and Ulysses spacecraft (Grün et al. 1992a,b). The sensor aperture was an approximate square with dimension  $124 \times 115\text{ mm}^2$ . A detailed description of the sensor was given by Igenbergs et al. (1998) and Senger (2007), and the calibration of the instrument was described by Naumann (2000). A sketch of the Nozomi spacecraft showing the MDC instrument is shown in Figure 4, and its detection geometry is described in Section 3.2.

### 3.2 MDC Sensor Pointing Direction

A fundamental parameter for the interpretation of dust measurements is the sensor pointing direction during a dust particle impact, in addition to the orbital position of the spacecraft. MDC was mounted onto the spacecraft body of Nozomi at an angle of  $135^\circ$  from the antenna pointing direction, as can be seen in Figure 4. The spacecraft was spin-stabilised, rotating about the antenna axis with a rotation period of approximately 7 to 10 revolutions per minute. Most of the time when the spacecraft was in interplanetary space, the antenna pointed towards Earth for communication purposes so that MDC

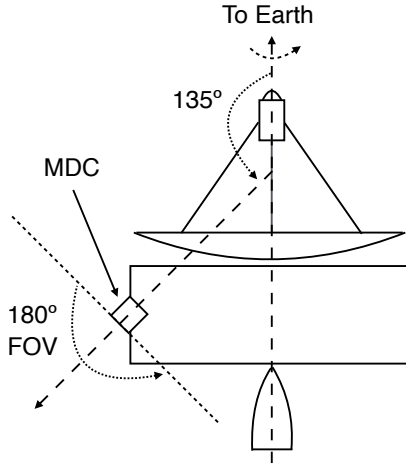


Figure 4. : Orientation of the Nozomi spacecraft and the MDC. The antenna (top) pointed towards Earth most of the time during the interplanetary mission phase, and MDC largely faced the anti-Earth hemisphere. The sensor axis had an angle of  $135^\circ$  from the antenna pointing direction. During one spin revolution of the spacecraft the sensor axis scanned an angle of  $90^\circ$ . MDC itself had almost  $180^\circ$  field of view (FOV).

largely faced the anti-Earth hemisphere. Due its large field of view (FOV), the sensor scanned the entire anti-Earth hemisphere during one spacecraft revolution, including the region around the ecliptic poles. The antenna pointing direction in ecliptic coordinates is shown in Figure 12 in the Appendix. It shows that during the early mission phase when the spacecraft was in Earth orbit, the antenna pointing varied significantly due to frequent spacecraft attitude changes and orbital manoeuvres, and Earth and Moon swing-bys.

In Figure 5 we show the deviation of the spacecraft rotation axis from the nominal Earth direction during the interplanetary mission of Nozomi. Most of the time the axis pointed within  $5^\circ$  of the Earth direction. This rather small deviation is negligible for the considerations and the interpretation of dust measurements in this paper.

### 3.3 Detection Geometry

MDC was mounted at an angle of  $135^\circ$  from the antenna pointing direction (cf. Figure 4). Thus, the sensor axis scanned an angle of  $90^\circ$  during one revolution of Nozomi. MDC itself with its box-like shape had almost  $180^\circ$  FOV (Senger 2007). Due to the rectangular sensor design, the effective sensor area to

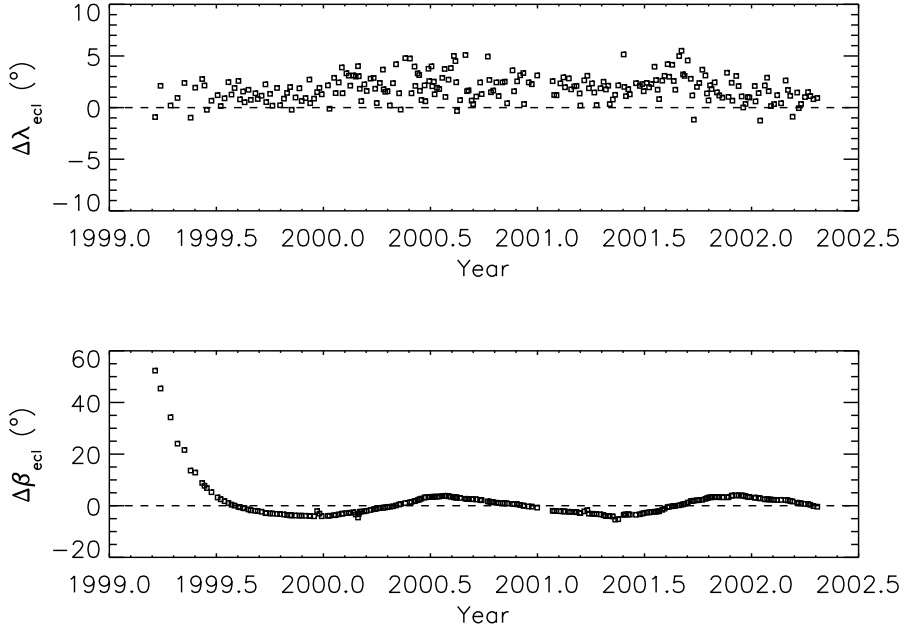


Figure 5. : Spacecraft attitude: deviation of the antenna pointing direction (i.e. positive spin axis) from the nominal Earth direction during the interplanetary mission of Nozomi. The deviations are given in ecliptic longitude  $\Delta\lambda_{\text{ecl}}$  (top) and latitude  $\Delta\beta_{\text{ecl}}$  (bottom, equinox J2000).

some extent depends on the particle impact direction. In addition, the spacecraft body, other instruments and a solar panel mounted close to MDC obscured the MDC's FOV. Furthermore, the penetrability of the entrance grid depends on the particle size and the impact direction (Section 3.1). The effective sensitive area of MDC must take these obscuring structures into account. The resulting average sensitivity profile of MDC w.r.t. the negative spacecraft spin axis, i.e. the anti-Earth direction, is shown in Figure 6.

### 3.4 Instrument Operation

Soon after launch, the MDC became operational and provided its first data. The failure of the power supply unit on 24 April 2002 (Section 2; Forbes et al. 2005) terminated the operation of all scientific instruments on board, including MDC. Nevertheless, the instrument provided dust measurements in the Earth environment and in the interplanetary space between Earth and Mars almost continuously for a total of approximately 3 years and 8 months.

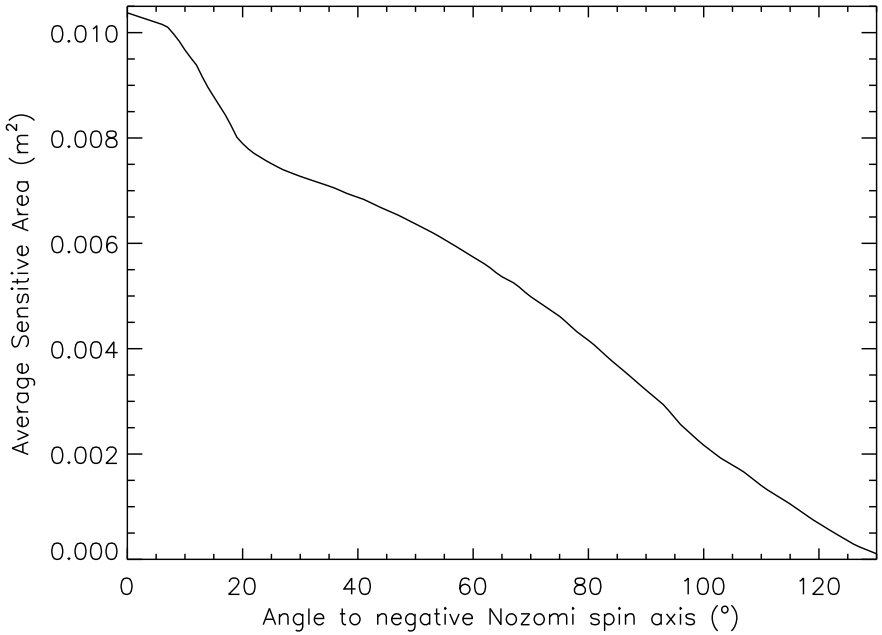


Figure 6. : MDC sensitivity profile during one spin revolution of the spacecraft, adapted from Senger (2007). The positive spacecraft spin axis pointed close to the Earth direction during the interplanetary mission phase (Figure 5).

### 3.5 Instrumental Noise and Dead Time

The MDC recorded a large number of noise events that may have affected the instrument's detection capabilities, given that every single signal triggered and processed by the MDC electronics causes some instrument dead time and may therefore affect the analysis of the dust data. The effects and characteristics of the recorded noise rate and noise signals are discussed in detail by Senger (2007). Here we give only a brief summary.

The noise events were either discarded by the flight software onboard and can only be recognised by the instrument's noise counter, or passed the onboard noise recognition scheme and can be seen in the data transmitted to Earth. Many of these noise signals were not shaped randomly as it is expected for noise caused by random electromagnetic background from different possible sources like radiation or the spacecraft's electrical systems. Rather, several nearly identical signal shapes were identified which occur in certain patterns. In addition to the signal shape, the coincidences, i.e. delay times, between individual charge signals as well as the charge amplitudes are critical parameters for the separation between dust impacts and noise.

A significant source of noise was due to the release of electrons caused by photo-ionisation at the inner MDC sensor box surfaces due to solar ultraviolet photons. It was a function of the spacecraft orientation and occurred when the Sun was illuminating the inner sensor box. The Sun could shine into the sensor box when the angle between the Nozomi rotation axis and the direction towards the Sun was larger than  $45^\circ$  (cf. Figure 4). This happened mostly early in the mission when the spacecraft was orbiting the Earth, while for most of the interplanetary mission after spring 1999, this angle was below  $45^\circ$ , and the noise usually remained low.

Nevertheless, several additional periods of very high noise rates occurred during the interplanetary mission phase when the Sun could not illuminate the inner sensor walls. The origin of these sporadic interferences remains unclear. Solar eruptions were considered as possible sources since such events cause very high proton fluxes and, therefore, may be recorded as noise events by MDC, similar to the one that occurred on 24 April 2002 and was the likely cause of the Nozomi failure. However, no additional coincidences between periods of high noise rates recorded by MDC and other known solar eruptions could be found. Other potential sources of strong noise like the Nozomi electronics itself were not examined due to missing information (Senger 2007).

Given that the high noise rates may have affected the detection capabilities for dust impacts, Senger (2007) determined the total detector dead time during the most significant noise periods. The highest detector dead time derived for the entire mission including the Earth orbiting phase reached a value of 14.5% and occurred only once, namely on 8 November 1999 for about six hours. During the other high noise periods the detector dead time varied between less than 1% and nearly 6% (these values occurred during the time periods 6 to 14 June 1999, 8 to 28 Nov. 1999, 22 Aug. to 28 Nov. 2000 and 16 Aug. 2001, respectively). During the remaining more than 90% of the mission time the overall dead time was significantly below 1%. In summary, the dead time caused by high noise rates is negligible for our analysis.

Even though the noise rates were very high during some intermittent periods and the total number of noise events detected during the entire mission exceeded 20,000, it is expected that the number of erroneously discarded real dust impacts is low (see also Section 4.2). Unfortunately, this value cannot be quantified because the original raw data of MDC and the noise events discarded by the noise identification scheme are not available anymore. Only the processed dust data presented in Tables 1 to 3 are still available today.

## 4 Dust Impact Events

In this Section we give an overview of the dust measurements of MDC on board Nozomi. We extracted the MDC dust data set from the thesis of Senger (2007). The data set is given in Tables 1 to 3 in the Appendix (R. Senger's thesis also contains graphs showing the charge signal curves measured for each identified dust impact which were not extracted from the thesis and not digitised). An electronic version of the MDC data is available at

[http://dpsc.perc.it-chiba.ac.jp/data/publication/krueger2026/krueger2026\\_NOZOMI\\_MDC\\_data.txt](http://dpsc.perc.it-chiba.ac.jp/data/publication/krueger2026/krueger2026_NOZOMI_MDC_data.txt),

and can also be obtained from the first author of this publication upon request.

### 4.1 Dust detections in Earth Orbit

The Earth orbiting phase of Nozomi lasted from launch on 3 July 1998 UT until the Earth swing-by on 20 December 1998. About 10,000 signals were triggered by the MDC electronics, recorded, qualified by the on-board software and transmitted to Earth (Senger 2007). 20 good signals were identified as dust impacts by manual screening. For one of them a correct determination of the charge rise time and amplitude was not possible and, thus, no impact speed and particle mass could be derived. Figure 1 shows the Nozomi orbit during the Earth-orbiting phase with superimposed positions where the particle impacts were detected. Note that all particles were detected far away from the Earth near the apogee of Nozomi. This will be discussed further in Section 5.

### 4.2 Dust Detections in Interplanetary Space

After leaving the Earth orbit on 20 December 1998, Nozomi was on a heliocentric orbit with perihelion at 1.0 AU and aphelion at 1.44 AU, close to Mars' orbit. The MDC was in operation during the entire mission time in interplanetary space until the system failure occurred on 24 April 2002 (cf. Section 2). Nozomi completed 3 1/2 orbits around the Sun and detected interplanetary and interstellar dust particles. About 11,000 signals were triggered, recorded, qualified and their data sets downloaded during the interplanetary mission phase.

In order to separate noise events from potential signals of real dust impacts, a neural network was used for pattern recognition. It was used to create a procedure that recognises real impact signals and separates

them from noise signals produced by the MDC sensor. The input parameters must represent the overall characteristics of the signal in a unique way. For an optimized performance of the pattern recognition process, the number of input parameters should be minimized and any redundancies should be avoided. The network itself should be as slim as possible in order to reduce the required computing power, and the number of events that are falsely identified as real impacts should be minimal. The desired output for the given problem reduces to a simple "yes/no" answer, i.e. either the presented signal is identified as a real impact signal or not. As input parameters, the signal itself or the whole set of digitized data, respectively, was not concerned as a practical approach since that would require more than 800 input neurons and lead to a very huge neural network. Instead, a set of 56 parameters that represent the characteristics of the signal was used as initial set of input parameters. These parameters include a reduced set of data points of the signals, and calculated parameters like the mean pre-trigger or total amplitude of the signal. In a first approach, the network was designed quite large, using all the 56 input parameters that describe the signal shape. The parameters were subject to optimisation that was performed by implementing different possible networks and evaluating their classification capabilities. Although this network showed only a weak classification performance, it was used as a basis for the following optimizations. The number of input parameters was reduced to the 16 most significant parameters and 2 output parameters. There were several different topologies of the neural network which could be conceived. All possible and reasonable topologies were implemented, trained and validated in order to carry out a systematic determination of the best performing network topology. As the same network shows different performance for each new created instance, 5 runs for each topology were made to get a significant average. A training goal of 0.01, i.e. an accuracy of higher than 99% in classification performance, was reached. (see Senger 2007, for details). In total, 76 dust impacts were extracted from the data measured in interplanetary space. For 16 of them no speed and mass determination was possible. The locations where the particles were recorded during Nozomi's interplanetary mission are shown in Figure 2.

## 5 Analysis

In this Section we perform an analysis of the Nozomi MDC dust measurements. We concentrate on the instrument's raw data measured for each detected dust impact, i.e. particle impact speed, mass, impact direction, and derived dust flux. We also perform a comparison with interplanetary dust detections

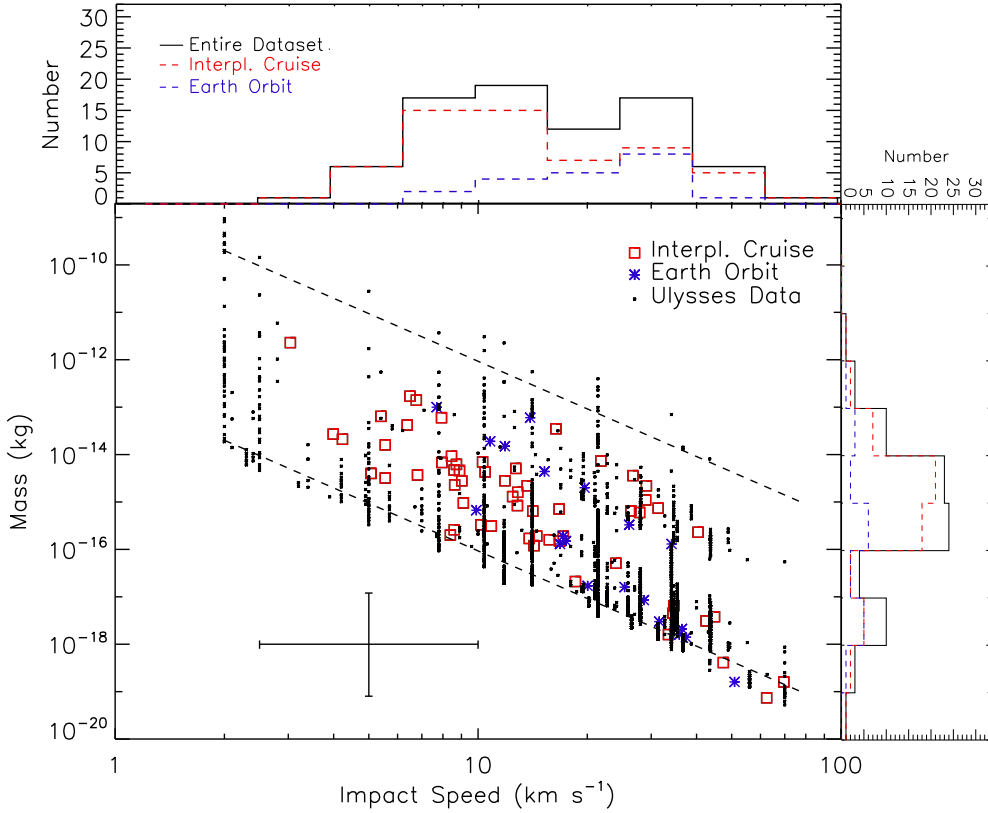


Figure 7. : Particle mass vs. impact speed of the dust particles measured with MDC. Ulysses data are shown for comparison (Krüger et al. 2010). The detection limits for MDC are shown as dashed lines. They are mean values for all impact positions inside the MDC sensor box (Senger 2007). A sample error bar is shown that indicates a factor of 2 uncertainty for the impact speed and a factor of 10 for the mass determination. Projections of the MDC data onto the mass and speed axes are shown as histograms (see also Figures 9 and 10).

obtained with the Ulysses spacecraft (Krüger et al. 2010). Our analysis presented here supplements the work presented by Senger (2007).

### 5.1 Dust Mass versus Impact Speed

In Figure 7 we show the measured impact speeds and particle masses for all 79 dust particles with available impact speed and mass measurement identified in the MDC data set (Senger 2007). Impact speeds occur over almost the entire calibrated range of the instrument from  $3 \text{ km s}^{-1}$  to  $70 \text{ km s}^{-1}$ . The

particle masses vary over more than 7 orders of magnitude from approximately  $10^{-12}$  kg to  $10^{-19}$  kg. The uncertainties are a factor of 2 for the speed and a factor of 5 for the mass (Naumann 2000).

For comparison, we also show the data measured with the dust detector onboard the Ulysses spacecraft which was an impact ionisation detector of a similar design (Grün et al. 1992b). Because the sensitive area of the Ulysses detector was by a factor of ten larger than that of the MDC, and the operation time was much longer, Ulysses recorded a much higher number of particle impacts. From 16 years of dust measurements between 1990 and 2007, the data sets of 6719 dust impacts onto the Ulysses sensor were transmitted to Earth (Krüger et al. 2010).

The clustering in the speed values of the Ulysses data is due to discrete steps in the charge rise time measurement but this quantisation is much smaller than the uncertainty in the speed measurement (due to the discrete digitisation steps in the charge and the rise time measurement of the Ulysses instrument, each dot in Figure 7 usually corresponds to more than one dust impact.). Figure 7 shows that at high impact speeds above approximately  $20\text{ km s}^{-1}$  the dust instruments on board both spacecraft had similar sensitivities for dust impacts. For lower speeds the Ulysses detector was a factor of 5 to 10 more sensitive in particle mass. It is also obvious that the mass-velocity dependence of the MDC was somewhat steeper than that of the Ulysses detector, as can be seen when comparing the lower boundaries of the Ulysses and the MDC data in Figure 7. These variations may be related to differences in the instrument electronics, detector geometry or other reasons. The details, however, cannot be investigated anymore 30 to 40 years after the MDC and the Ulysses dust instruments were manufactured.

The 20 particles detected by MDC in Earth orbit with measured impact speed and particle mass are highlighted as asterisks in Figure 7. The lowest impact speed was  $7.7\text{ km s}^{-1}$ , and the highest was  $50.9\text{ km s}^{-1}$ . From the measured impact speed and Nozomi's orbital and attitude data, Senger (2007) derived the heliocentric speed of all detected particles (Tables 1 to 3). For the particles measured in Earth orbit, the derived heliocentric speeds range from 17 to  $67\text{ km s}^{-1}$ . This is much higher than the escape speed from Earth's gravitational field at the geocentric distance where the particles were measured. Therefore, all particles detected during the first half year of the Nozomi mission must have been unbound to the Earth system and, thus, be of interplanetary or interstellar origin. This is in agreement with the dust measurements by Hiten during its three year mission in the Earth-Moon system, which was equipped with a similar dust sensor (Iglseder et al. 1993; Svedhem et al. 1996). Thus, the Nozomi MDC neither detected dust particles of natural origin that were bound to the Earth nor manmade space debris.

## 5.2 Dust Impact Rate

The dust impact rate detected by the Nozomi MDC from July 1998 until April 2002 is displayed in Figure 8. The highest overall impact rate of approximately  $1.5 \times 10^{-6} \text{ s}^{-1}$  was detected during the Earth orbiting phase between July and December 1998. During the initial interplanetary mission phase in 1999 and early 2000 the impact rate was about a factor of 3 lower, increased to about  $1 \times 10^{-6} \text{ s}^{-1}$  again in mid-2000, and stayed rather constant at this level until the end of the MDC operations in April 2002.

In order to compare the Nozomi dust measurements with theoretical predictions by an interplanetary dust model, we simulated the Nozomi measurements with the Interplanetary Meteoroid Engineering Model (IMEM; Dikarev et al. 2005a,c). We assumed the MDC sensor profile shown in Figure 6, and the Nozomi antenna axis pointing shown in Figure 12 in the Appendix. Given that the spacecraft rotation axis pointed close to the Earth direction after mid 1999, the MDC scanned the anti-Earth hemisphere most of the time in this period.

The dashed line in Figure 8 shows the expected dust impact rate for Nozomi MDC derived from the IMEM model. For the simulations we assumed a detection threshold of MDC of  $1.5 \times 10^{-16} \text{ kg}$  in order to get a reasonable fit of the measured impact rate. It corresponds to an average dust impact speed of approximately  $10 \text{ km s}^{-1}$  (cf. Figure 7), and it is in overall agreement with the impact speeds measured by MDC (Figure 9). The upper limit of the size range considered in the simulations is  $10^{-2} \text{ kg}$ . Due to the steep dust size distribution falling off with increasing particle size, the choice of this latter value has no influence on the modelling results. In order to assess the influence of the selected minimum mass on the predicted flux, we ran the IMEM model with different mass thresholds. This showed that a factor of 2 increase or decrease in the lower mass cutoff changes the average predicted flux by a factor of 1.3, a factor of 5 change in the mass cutoff changes the flux by a factor of 2, and a factor of 10 change in the mass cutoff leads to a factor of 2.6 change in the flux, respectively. The simulations were performed with a time step of 1 day, and gravitational focussing of interplanetary dust by the Earth was taken into account in 1998 when Nozomi was in Earth orbit.

The strong fluctuations in the simulated impact rate in 1998 are caused by frequent changes in the spacecraft attitude. On the other hand, the variation of the dust impact rate predicted by the IMEM model for the interplanetary mission by almost a factor of two is mainly caused by the variation in the dust spatial density and impact speed between the orbits of Earth and Mars, and by the changing sensor

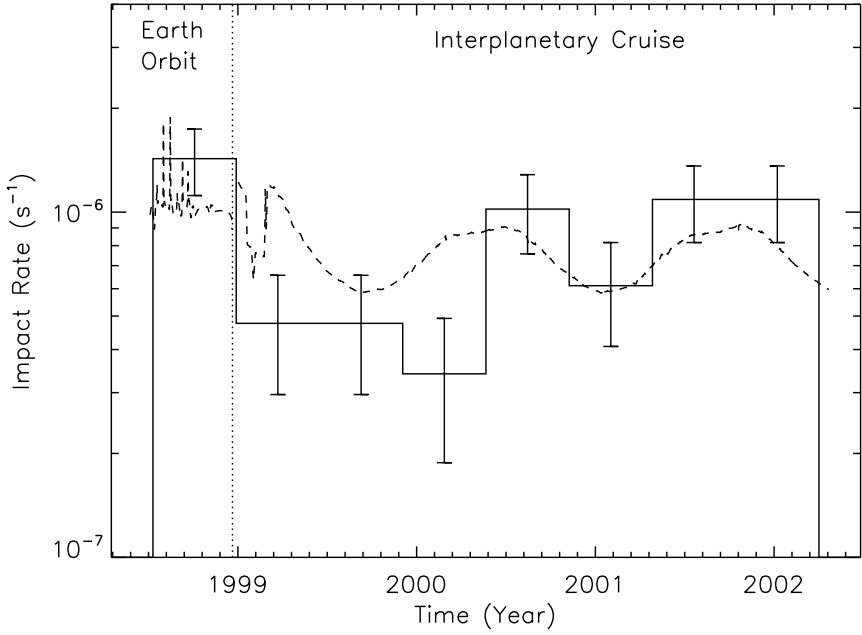


Figure 8. : Dust impact rate measured by Nozomi MDC. The second Earth flyby on 20 December 1999 and subsequent entry into the interplanetary trajectory is shown as a vertical dotted line. The error bars indicate the  $\sqrt{N}$  variation with  $N$  being the number of dust impacts in the respective time bin. The dashed line shows the approximate flux of interplanetary dust particles as derived from the IMEM model, see text for details.

orientation w.r.t. the dust flow.

The impact rate predicted by the model is in overall agreement with the MDC measurements, although the model predicts a smaller variation of the impact rate than is actually seen in the data. Here the relatively low number of measured particles in each time bin may have an influence. The measured impact rate and the IMEM model will be discussed further in Section 6.1.

### 5.3 Impact Speed Distribution

In Figure 9 we show the impact speed distribution of the dust impacts measured by Nozomi MDC. The average impact speed of the 20 particles measured in Earth orbit is approximately  $23 \pm 11 \text{ km s}^{-1}$ , while that of the 80 particles detected in interplanetary space is about  $19 \pm 15 \text{ km s}^{-1}$ . Given that the motion of particles detected in Earth orbit is affected by the gravitational attraction of the Earth, they should have higher average impact speeds than particles detected in interplanetary space. Thus, the increased

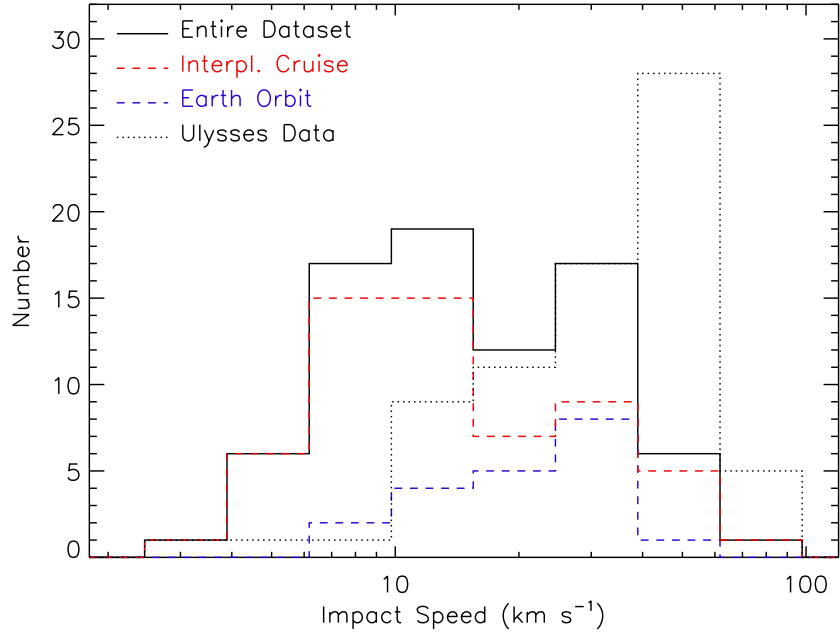


Figure 9. : Impact speed distribution for the dust impacts measured by Nozomi MDC. The speed distribution measured with the Ulysses dust detector in 1990 between 1 and 1.45 AU (73 dust impacts) is shown for comparison.

measured impact speeds in Earth orbit are in qualitative agreement with this expectation, although this is not statistically significant.

Figure 9 shows a few impacts with speeds exceeding approximately  $40 \text{ km s}^{-1}$ . The escape speed from the gravitational attraction of the Sun at the heliocentric distance of Nozomi (1.0 to 1.44 AU) ranges from  $42 \text{ km s}^{-1}$  to  $35 \text{ km s}^{-1}$ . Thus, based on the measured impact speeds, these high speed particles are good candidates for particles being unbound to the solar system. We will come back to this in Section 6.2.

Figure 9 shows the speed distribution measured with the Ulysses dust detector for comparison (Grün et al. 1995). We only show the Ulysses data measured in the distance range between 1 and 1.45 AU in the year 1990. (We used 73 Ulysses detections between launch on 6 October and 20 December 1990 when the spacecraft was in the heliocentric distance range between 1 AU and 1.45 AU, with measured impact speeds and particle masses and a velocity error factor  $\text{VEF} < 10$  (Krüger et al. 2010).). The average impact speed of the 73 particles measured with Ulysses in this time interval is  $36 \pm 17 \text{ km s}^{-1}$  and, thus, much higher than the impact speeds measured with Nozomi MDC in a comparable region of space (60 particles with  $19 \pm 16 \text{ km s}^{-1}$ ). The average impact speed predicted by the IMEM model for the MDC

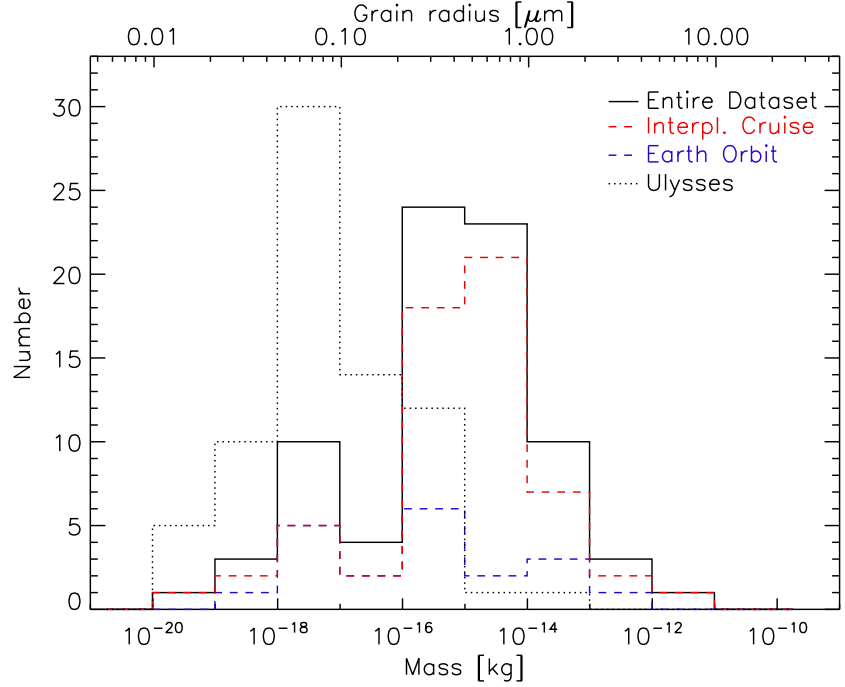


Figure 10. : Mass distribution for the dust impacts measured by Nozomi MDC. The mass distribution measured with the Ulysses dust detector in 1990 between 1 and 1.45 AU (73 dust impacts) is shown for comparison. The corresponding radius for spherical particles with density  $2,500 \text{ kg m}^{-3}$  is shown at the top.

measurements is about  $12 \text{ km s}^{-1}$ , in agreement with the measurements. This is consistent with the fact that Ulysses, heading towards Jupiter on a direct trajectory, traversed this region of space with a much higher speed than Nozomi which had its aphelion at Mars' orbit, leading to higher impact speeds in the case of Ulysses.

#### 5.4 Mass Distribution

In Figure 10 we show the mass distribution of all 79 particle impacts for which the impact speed and particle mass are available, again separate for the Earth orbiting phase and the interplanetary mission phase of Nozomi. Below approximately  $10^{-15} \text{ kg}$  the mass distribution is incomplete because the detection threshold varies with the impact speed (see Figure 7). High impact speeds lead to a detection threshold shifted towards smaller particles and vice versa. Furthermore, the detection threshold of the instrument is not a fixed and well-defined value but rather a range in impact charge. This was also seen in the Ulysses and Galileo dust instrument data (e.g. Krüger et al. 2010, their Fig. 4).

The mass distribution measured with Ulysses shows a maximum at two orders of magnitude lower masses than the one measured with Nozomi. This is overall consistent with the higher impact speeds measured with Ulysses (Section 5.3), given that the detection threshold  $m_{\text{thr}}$  of impact-ionisation dust detectors is a strong function of the impact speed  $v_{\text{imp}}$ :  $m_{\text{thr}} \approx v_{\text{imp}}^{-3.5}$  (Göller and Grün 1985; Auer 2001, see also Figure 7). Thus, an increase in impact speed by a factor of 2 shifts the detection threshold to approximately a factor of 10 smaller particle masses. Assuming that Nozomi and Ulysses detected the same dust populations and had comparable detection thresholds, this partially explains the maximum in the Ulysses measurements at lower masses. The other factor of 10 shift is likely due to a more sensitive detection threshold of the Ulysses sensor at impact speeds below approximately  $10 \text{ km s}^{-1}$ , as is indicated in Figure 7.

## 5.5 Impact Direction

Senger (2007) derived particle velocity vectors in heliocentric coordinates for all 79 particles for which the impact speed and impact direction were measured (Tables 1 to 3). The velocity vector converted to heliocentric ecliptic coordinates is shown in Figure 11.

In his thesis, Senger (2007) discussed neither the uncertainties in the determination of the particle velocity vector nor in the particle's orbital elements. The matter is complicated because of the complex FOV of MDC. Due to the box shape of MDC and its inclined mounting orientation on board Nozomi, and spacecraft structures obscuring the FOV, the accuracy depends on the direction (note that the sensitivity profile in Figure 6 shows an average over all directions). Senger gives a range of  $0.77 \pi \text{ sr}$  to  $0.83 \pi \text{ sr}$  with an average of  $0.81 \pi \text{ sr}$  for the sensitive solid angle of MDC. This also illustrates the wide FOV of MDC which inevitably leads to large uncertainties in the reconstructed particle trajectories. Unfortunately, Senger (2007) did not give an estimate of the accuracy of the particle trajectories. According to Grün et al. (2001, page 314) the dust detector on board the Hiten spacecraft could determine the trajectory of individual dust particles with  $\pm 75^\circ$  accuracy. Given the very similar sensor designs of both the Hiten and Nozomi instruments, and ignoring differences in the mounting configuration and the obscuration pattern, we can assume a similar accuracy for the trajectory determination for Nozomi MDC. This large uncertainty in the trajectory determination illustrates the necessity for dust instruments with a much better spatial resolution like the DESTINY<sup>+</sup> Dust Analyzer (DDA; Simolka et al. 2024) in order to

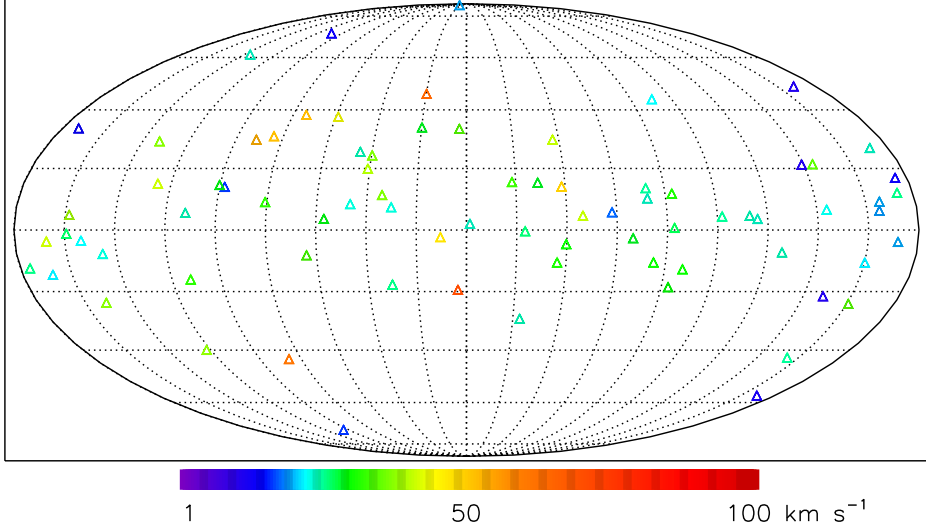


Figure 11. : Dust impact directions in ecliptic coordinates showing the flow directions (downstream) at the location of Nozomi of the 79 dust particles measured by MDC with derived mass and impact speed (cf. Tables 1 to 3). Each triangle denotes a dust particle impact. The colour code reflects the particle's derived heliocentric speed at the location of the spacecraft where the particle was detected.  $0^\circ$  ecliptic longitude is to the left.

provide a much improved determination of the dust particle trajectories (cf. Section 6.4).

The particle distribution shows a concentration towards the ecliptic plane which is expected if the majority of the particle detections is of interplanetary or interstellar origin. The distribution of the particle impacts over the overall range in ecliptic longitudes tends to be rather smooth. To first order, this is a function of the overall sky coverage of the MDC FOV during the entire mission time. A detailed analysis showed that the entire sky was covered well by MDC with maximum and minimum coverage deviating by only about 50% from the average value (Senger 2007). Thus, a rather smooth distribution of particle impacts with ecliptic longitude can be expected.

## 6 Discussion

In the previous Sections we presented an overview and a re-analysis of the in situ dust measurements obtained by the MDC on board Nozomi in Earth orbit and in interplanetary space. In this Section we

briefly discuss the results for three identified dust populations: interplanetary dust, interstellar dust, and dust detections during the Nozomi crossing of the Geminids meteoroid stream.

## 6.1 Interplanetary Dust

Very likely about 95% of the 79 particles with measured mass and impact speed detected by Nozomi MDC are of interplanetary origin (see also Section 6.2). This also applies to the particles detected in Earth orbit.

We have used the IMEM model to simulate the Nozomi measurements (cf. Section 5.2). The model was calibrated with infrared observations of the zodiacal cloud by the Cosmic Background Explorer (COBE) DIRBE instrument, in situ flux measurements by the dust detectors on board the Galileo and Ulysses spacecraft, and the crater size distributions on lunar rock samples retrieved by the Apollo missions. The model considers the orbital distributions of a number of known sources, including the asteroid belt, as well as comets on Jupiter-encountering orbits (Dikarev et al. 2004, 2005a,b,c). In order to calculate the particle dynamics, solar gravity and the velocity-dependent tangential component of radiation pressure (Poynting-Robertson effect) are taken into account, while the radial component of solar radiation pressure and the electromagnetic interaction of electrically charged dust particles are neglected. Given that the IMEM model was calibrated with the Ulysses and Galileo in situ dust measurements, among other data sets, and that the model gives overall good agreement with the Nozomi MDC measurements, we conclude that the Nozomi and the Ulysses/Galileo measurements are in overall agreement. The agreement between the MDC measurements and the IMEM model also indicates that the noise identification scheme applied by Senger (2007) is rather reliable. In particular, a large fraction of unrecognised noise events in the data set or, vice versa, too many real dust impacts discarded by the noise identification scheme, would lead to significant disagreement with the model predictions.

The so-called apex particles are a population of the interplanetary dust flux that are expected to orbit in nearly circular orbits with a lower circular speed than macroscopic objects due to the effect of radiation pressure. In order to produce sufficiently large impact charge signals and be detectable by MDC and similar impact ionisation dust sensors the particles should impact the sensor with a minimum of  $3 \text{ km s}^{-1}$  (Grün et al. 1992a,b) which is thus an approximate value for the speed difference of the particles. Because of this lower speed, such particles are expected to impact preferably from the apex direction of the

spacecraft. Senger (2007) pointed out that the effective sensitive area of MDC for interplanetary particles approaching from the apex direction of Nozomi was approximately an order of magnitude lower between mid-1999 and mid-2000 than later in the mission. Thus, the minimum in the impact rate in 1999 and early 2000 (Figure 8) may be related to the drop of the sensitive area in this time period, and the fact that radiation pressure is not fully included in the IMEM model.

The speed distribution of the particles detected by MDC during Nozomi's Earth orbiting phase is similar to the one measured by the nearly identical dust detector on board the Hiten spacecraft which was also in Earth orbit (Senger 2007, not shown here). In both cases the derived *geocentric* speeds are in excess of the local escape speed from the Earth gravitational field, indicating that by far the majority of the detected particles were unbound to the Earth system. Thus, Nozomi and Hiten likely detected similar populations of particles entering the Earth system from interplanetary space.

Figure 1 may suggest that there is a concentration of particle detections around the orbit of the Moon, indicating a potential dust ring around the Earth at the distance of the Moon. However, Senger (2007) pointed out that this cannot be the case because of the derived high particle speeds which imply particle orbits unbound to the Earth system. Furthermore, no increase in the detection rate was registered during the two lunar swingbys.

## 6.2 Interstellar Dust

In our local environment, the Sun and the heliosphere are surrounded by the Local Interstellar Cloud (LIC) of warm diffuse gas and dust where dust is assumed to contribute about 1% to the cloud mass (Mann 2010; Kimura 2015; Krüger et al. 2015). The Sun's motion with respect to this cloud causes an inflow of interstellar matter into the heliosphere (Frisch et al. 1999). After initial predictions based on zodiacal light measurements in the 1970s (Bertaux and Blamont 1976; May 2007), measurements with the dust detectors on board the Ulysses and Galileo spacecraft showed that a collimated stream of interstellar dust passes through the Solar System due to the Sun's motion relative to the LIC (Grün et al. 1993; Baguhl et al. 1995). The measured heliocentric speed of the dust flow is approximately  $26 \text{ km s}^{-1}$  (Grün et al. 1994; Krüger et al. 2015) and its flow direction is compatible with the measured direction of the inflowing interstellar neutral helium gas ( $\lambda_{\text{ecl}} = 75.4^\circ$  and  $\beta_{\text{ecl}} = -5^\circ$  downstream; Witte 2004; Strub et al. 2015; Swaczyna et al. 2023).

Even though most of the particles detected in interplanetary space by Nozomi MDC were interplanetary dust orbiting the Sun, MDC also detected several particles of interstellar origin. From the analysis of the impact speed and the impact direction and derived heliocentric particle trajectories, Sasaki et al. (2007) and Senger (2007) independently identified 3 and 5 interstellar particle candidates, respectively.

Assuming an average of four particle impacts measured from 1999 to 2002, and considering the detection geometry of MDC for interstellar dust during this time period, we get an interstellar dust flux of approximately  $10^{-5} \text{ m}^{-2} \text{ s}^{-1}$  with roughly a factor of 5 uncertainty. Given that the interstellar particles have expected impact speeds in excess of approximately  $20 \text{ km s}^{-1}$  this value refers to particles with masses above  $10^{-17} \text{ kg}$  (cf. Figure 7). This value is in overall good agreement with interstellar dust fluxes measured with in situ impact-ionisation dust detectors carried by other space missions in the solar system (Hitenn, Helios, Ulysses, Galileo, Cassini; Svedhem et al. 1996; Krüger et al. 2019).

The value derived from the MDC measurements is also in agreement with the dust fluxes derived from the interstellar dust collections performed with the Stardust spacecraft en route to comet 81P/Wild (also known as Wild 2). In addition to its main objective, namely the collection of cometary particles during the flyby at comet 81P, Stardust also carried silica aerogel collectors dedicated to the collection of interstellar particles. The collectors were exposed to the interstellar dust flow for 195 days in two periods in 2000 and 2002. Seven dust particles were captured in the dust collectors and analysed on Earth (Westphal et al. 2012). The estimated flux of these particles which have approximately  $1 \mu\text{m}$  diameter is  $2 \times 10^{-6} \text{ m}^{-2} \text{ s}^{-1}$ . This value is in overall agreement with the flux derived from the MDC, in particular when considering that these values were derived with very different measurement techniques, namely impact ionisation detection and visual inspection of the aerogel, respectively. A detailed re-analysis of the interstellar particle detections by Nozomi MDC is beyond the scope of this paper. In connection with dust dynamical simulations, it will be the subject of a future publication.

### 6.3 Cometary Dust Trails

When a comet approaches the Sun, sublimating gases carry solid particles away from the comet's surface. Solar radiation pressure quickly moves the small sub-micrometre sized particles away from the comet nucleus, and the particles form the comet's dust tail. Larger dust particles with sizes exceeding approximately  $10 \mu\text{m}$  are ejected from the cometary nucleus at lower speeds and remain very close to

the comet orbit for several revolutions around the Sun (Soja et al. 2015). They slowly spread along the comet's orbit as a result of small differences in orbital period, forming a tubular structure along the orbit of the parent comet filled with dust. These structures are called meteoroid streams or dust trails. When the Earth intercepts a cometary trail, the particles can collide with the atmosphere and show up as meteors and fireballs, generating a meteor shower.

On 18 November 1998 the Earth crossed the trail of comet 55P/Tempel-Tuttle, leading to a very prominent meteor shower. For an observer on the Earth the apparent approach direction of the meteors (radiant) is from the constellation Leo and they are thus called the Leonids. Comet 55P/Tempel-Tuttle has a retrograde orbit so that the Leonid particles hit the Earth atmosphere with a high speed of around  $70 \text{ km s}^{-1}$ . Nozomi crossed the Leonid particle trail about 1 day after the maximum flux was observed on Earth.

Although the MDC high voltage was switched off during the encounter on 18 November, 4:00 UTC to avoid any damage of the instrument, four particle impacts were detected between 17 and 20 November 1998 that even show a correlation in approach direction. However, for all four particles neither the derived impact speed nor the particle approach direction fit to the Leonid dust stream (cf. Table 1). Instead, the detected particles approached approximately from the opposite direction. Thus, they cannot have directly originated from the Leonid dust trail. Nevertheless, a significant influence of the Leonid particle stream on the lunar sodium tail during the 1998 encounter was observed (Smith et al. 1999).

An asymmetric dust cloud surrounding the Moon was detected by the Lunar Dust EXperiment (LDEX) on board the Lunar Atmosphere and Dust Environment Explorer (LADEE) mission, and enhanced dust count rates were registered during periods when the Earth-Moon system crossed well-known meteor streams (Geminids, Northern Taurids, Quadrantids and Omicron Centaurids; Horányi et al. 2015; Szalay et al. 2018). Yang et al. (2022) studied the distribution of dust ejected from the lunar surface by hypervelocity impacts of micrometeoroids and the structure of the resulting steady-state dust cloud in the Earth-Moon system. Particles ejected from the lunar surface escape the gravity of the Moon, and they form an asymmetric torus between the Earth and the Moon in the geocentric distance range  $[10 R_E, 50 R_E]$  (mean Earth radius  $R_E = 6,371 \text{ km}$ ).

When considering the impacts measured by MDC at the time of the Leonids trail crossing around 18 November 1998, one has to consider Nozomi's distance from the Moon and the travel time of dust particles released from the lunar surface. During the crossing of the Leonids meteor stream Nozomi was far outside

the Earth-Moon system at a geocentric distance of approximately 1.6 million kilometres or approximately  $250 R_E$ . Thus, even for very high ejection speeds of  $1 \text{ km s}^{-1}$ , ejecta from impacts of Leonid particles onto the lunar surface would require approximately 9 days to reach Nozomi. This makes an explanation of the Nozomi detections by direct ejecta from the lunar surface unlikely. We therefore conclude that the detected impacts likely originate neither from the Leonid stream directly nor from impacts of Leonid meteoroids onto the lunar surface, and their origin remains elusive.

In order to search for particle impacts in the MDC data set detected during crossings of other cometary trails during the interplanetary mission of Nozomi, we performed a statistical analysis of the entire MDC data set comprising 96 particle impacts. The technique was described by Grün et al. (2001) and successfully applied to the measurements obtained with the Ulysses dust detector (Krüger et al. 2024), leading to the identification of a few likely cometary trail crossings of Ulysses. It turned out that due to the much lower number of particle detections as compared to Ulysses no statistical significant particle concentration could be identified in the Nozomi dust data.

#### 6.4 Future In Situ Dust Measurements

The negative outcome of the dust trail analysis described in the previous Section emphasises the necessity for large area dust detectors in order to derive statistically meaningful results from this kind of analysis. In the near future the Martian Moons eXploration (MMX) mission to the Martian moons Phobos and Deimos (Kuramoto et al. 2022) will be equipped with the Circum-Martian Dust Monitor (CMDM; Kobayashi et al. 2018). CMDM is a large area dust detector with  $1 \text{ m}^2$  sensor area. For dust detection the instrument will use the outermost polyimide film of the spacecraft multilayer insulation (MLI), which is a thermal blanket of the spacecraft. The sensor will use the MLI on one flat side of the spacecraft. Additionally, piezoelectric elements will be mounted on the MLI surface. A dust particle hitting or penetrating the MLI generates a stress wave that subsequently propagates through the MLI film and can be detected by one or more of the piezoelectric sensors. The MMX spacecraft is scheduled for launch in 2026, and the large area CMDM sensor will likely detect cometary dust trail particles en route to Mars (Krüger et al. 2021), as well as the predicted Martian dust ring.

Furthermore, the DESTINY<sup>+</sup> spacecraft – to be launched in 2028 – will be equipped with the DESTINY<sup>+</sup> Dust Analyzer (DDA; Simolka et al. 2024). DDA is an impact-ionisation time-of-flight mass spectrometer

with strong heritage from the Cassini Cosmic Dust Analyzer which very successfully measured dust throughout the Saturnian system (CDA; Srama et al. 2004, 2006, 2011). DDA has a sensitive area of  $0.03\text{ m}^2$ , i.e. it is three times larger than the Nozomi MDC. It will be equipped with a trajectory sensor to allow for the determination of the particle's velocity vector with an accuracy of about 10% for the impact speed and an angular accuracy of about  $10^\circ$ . This highly improved accuracy of the velocity measurement as compared to earlier instruments like, for example, the Ulysses dust detector or Nozomi MDC will open the possibility to trace each individual detected dust particle back to its source object, rather than relying on statistical techniques as applied in this work. Together with its improved particle composition measurement ( $m/\Delta m \approx 100 - 150$ , as compared to  $m/\Delta m \approx 30 - 50$  in the case of CDA), DDA will open a new window onto the composition and origin of the particles' source objects.

## 7 Conclusions

The Nozomi spacecraft, launched on 3 July 1998 UT, spent about six months in Earth orbit before being injected into an interplanetary trajectory. It traversed the spatial region between the orbits of Earth and Mars repeatedly, and the Mars Dust Counter (MDC) on board successfully measured interplanetary and interstellar dust until April 2002. A total of 96 dust impacts were extracted from the MDC data, 20 from the Earth orbiting phase and 76 from the interplanetary mission (Senger 2007).

We analysed the MDC data measured during each dust impact, i.e. particle impact speed, mass, impact direction, and derived dust flux. Furthermore, we compared the Nozomi results with in situ dust measurements obtained with the dust detector on board the Ulysses spacecraft (Krüger et al. 2010). Our analysis presented here supplements earlier work by Sasaki et al. (2007) and Senger (2007), and we make the Nozomi dust data set in electronic form available to the scientific community. Our results can be summarised as follows:

- Based on the measured particle impact speeds, all impacts detected when Nozomi was in Earth orbit must have been due to particles arriving from interplanetary space. Thus, while being in Earth orbit MDC detected neither dust particles of natural origin that were bound to the Earth nor space debris (Senger 2007).
- The dust impact rate measured in interplanetary space varied by approximately a factor of 2 and is overall consistent with theoretical predictions by the Interplanetary Meteoroid Engineering Model

(IMEM) model (Dikarev et al. 2005a,c).

- The particle impact direction was concentrated towards the ecliptic plane, consistent with the majority of the dust impacts being of interplanetary origin.
- The impact speeds and masses of dust particles measured by Nozomi MDC are overall consistent with the measurements obtained by Ulysses in the same region of space.
- No impacts of particles originating from cometary trails could be identified during known cometary trail crossings of Nozomi. A few impacts detected during the crossing of the dust trail of comet 55P/Tempel-Tuttle in November 1998 could not be assigned a cometary trail origin, and their origin remains elusive.

We expect that this review of the Nozomi dust measurements will be beneficial for future dust investigations with the upcoming Martian Moons eXploration (MMX) and DESTINY<sup>+</sup> space missions, to be launched in 2026 and 2028, respectively. Both missions will traverse the same region of space as Nozomi, and the MDC data, together with the Ulysses dust measurements, will likely serve as a valuable reference in the future.

## Acknowledgements

HK gratefully acknowledges support for a research visit at Planetary Exploration Research Center (PERC), Chiba Institute of Technology, Narashino, Chiba, Japan, where part of the work for this publication was done. The authors wish to thank Robert Senger for his comprehensive analysis of the Nozomi dust measurements published in his PhD thesis which formed the basis for the analysis presented in this paper. In particular, the Nozomi MDC dust data set, which is now available in electronic form, was extracted from the thesis. We thank two anonymous referees whose comments improved the presentation of our results.

## Appendix

The antenna pointing direction in ecliptic longitude and latitude is shown in Figure 12. The ecliptic latitude of the antenna pointing varied between approximately  $+55^\circ$  and  $-45^\circ$  during the first months of the mission and stabilised at  $+3^\circ$  for the rest of the mission time, while the longitude covered the entire range from  $0^\circ$  to  $360^\circ$ .

Tables 1 to 3 list the entire dust data set of Nozomi MDC extracted from the thesis of Senger (2007).

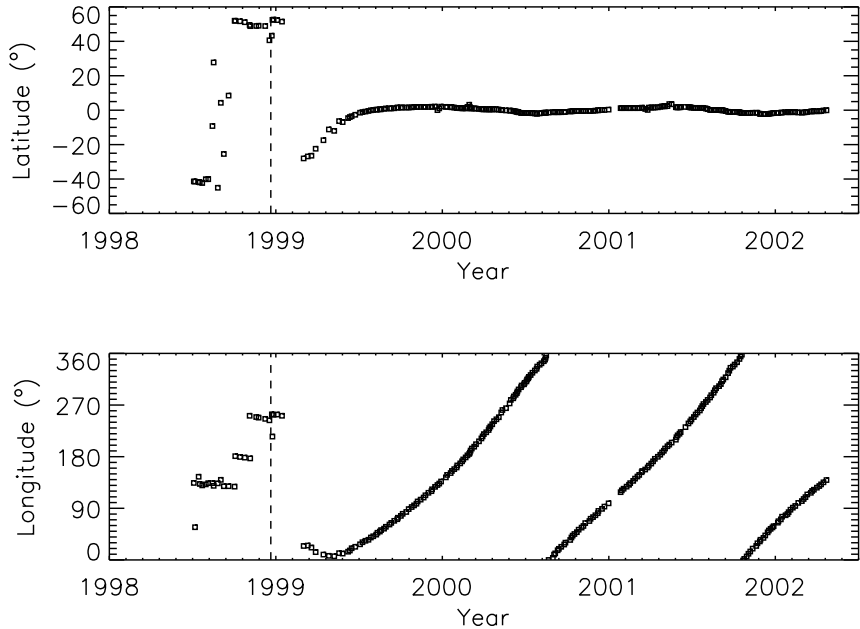


Figure 12. : Antenna pointing direction in ecliptic latitude (top) and longitude (bottom). The vertical dashed line shows the time when Nozomi left the Earth orbit. Adapted from Senger (2007).

## References

Arai, T., Destiny<sup>+</sup> Team, 2024. Current Status of DESTINY+ and Flyby Observation Plan of (3200) Phaethon, in: 55th Lunar and Planetary Science Conference, p. 1781.

Auer, S., 2001. Instrumentation, in: Grün, E., Gustafson, B.A.S., Dermott, S.F., Fechtig, H. (Eds.), Interplanetary Dust, Springer Verlag, Berlin Heidelberg New York. pp. 385–444.

Azzi, S., Oikonomidou, X., Lemmens, S., 2025. The space environment particle density in Low Earth Orbit based on two decades of in situ observation. *Advances in Space Research* 75, 6394–6405.

doi:10.1016/j.asr.2025.02.028, arXiv:2409.13794.

Baguhl, M., Grün, E., Hamilton, D.P., Linkert, G., Riemann, R., Staubach, P., 1995. The flux of interstellar dust observed by Ulysses and Galileo. *Space Science Reviews* 72, 471–476.

Bertaux, J.L., Blamont, J.F., 1976. Possible evidence for penetration of interstellar dust into the solar system. *Nature* 262, 263–266.

Dikarev, V., Grün, E., Baggaley, J., Galligan\*, D., Landgraf, M., Jehn, R., 2004. Modeling the Sporadic Meteoroid Background Cloud. *Earth Moon and Planets* 95, 109–122. doi:10.1007/s11038-005-9017-y.

Dikarev, V., Grün, E., Baggaley, J., Galligan, D., Landgraf, M., Jehn, R., 2005a. The new ESA meteoroid model. *Advances in Space Research* 35, 1282–1289. doi:10.1016/j.asr.2005.05.014.

Dikarev, V., Grün, E., Baggaley, W.J., Galligan, D.P., Landgraf, M., Jehn, R., 2005b. A single physical model for diverse meteoroid data sets. Technical Report. <https://arxiv.org/abs/1902.02977>.

Dikarev, V., Grün, E., Landgraf, M., Jehn, R., 2005c. Update of the ESA Meteoroid Model, in: Danesy, D. (Ed.), 4th European Conference on Space Debris, p. 271.

Forbes, J.M., Lu, G., Bruinsma, S., Nerem, S., Zhang, X., 2005. Thermosphere density variations due to the 15-24 April 2002 solar events from CHAMP/STAR accelerometer measurements. *Journal of Geophysical Research (Space Physics)* 110, A12S27. doi:10.1029/2004JA010856.

Frisch, P.C., Dorschner, J., Geiß, J., Greenberg, J.M., Grün, E., Landgraf, M., Hoppe, P., Jones, A.P., Krätschmer, W., Linde, T.J., Morfill, G.E., Reach, W.T., Slavin, J., Svestka, J., Witt, A., Zank, G.P., 1999. Dust in the Local Interstellar Wind. *Astrophysical Journal* 525, 492–516.

Göller, J.R., Grün, E., 1985. Calibration of the GALILEO/ISPM Dust Detectors with Iron Particles, in: Giese, R.H., Lamy, P. (Eds.), *Properties and Interaction of Interplanetary Dust*, Reidel, Dordrecht. pp. 113–115.

Grün, E., Baguhl, M., Divine, N., Fechtig, H., Hamilton, D.P., Hanner, M.S., Kissel, J., Lindblad, B.A., Linkert, D., Linkert, G., Mann, I., McDonnell, J.A.M., Morfill, G.E., Polanskey, C., Riemann, R., Schwehm, G.H., Siddique, N., Staubach, P., Zook, H.A., 1995. Two years of Ulysses dust data. *Planetary and Space Science* 43, 971–999.

Grün, E., Baguhl, M., Svedhem, H., Zook, H.A., 2001. In situ measurements of cosmic dust, in: Grün, E., Gustafson, B.A.S., Dermott, S.F., Fechtig, H. (Eds.), *Interplanetary Dust*, Springer Verlag, Berlin Heidelberg New York. pp. 295–346.

Grün, E., Fechtig, H., Hanner, M.S., Kissel, J., Lindblad, B.A., Linkert, D., Maas, D., Morfill, G.E.,

Zook, H.A., 1992a. The Galileo dust detector. *Space Science Reviews* 60, 317–340.

Grün, E., Fechtig, H., Kissel, J., Linkert, D., Maas, D., McDonnell, J.A.M., Morfill, G.E., Schwehm, G.H., Zook, H.A., Giese, R.H., 1992b. The Ulysses dust experiment. *Astronomy and Astrophysics*, Supplement 92, 411–423.

Grün, E., Gustafson, B.E., Mann, I., Baguhl, M., Morfill, G.E., Staubach, P., Taylor, A., Zook, H.A., 1994. Interstellar dust in the heliosphere. *Astronomy and Astrophysics* 286, 915–924.

Grün, E., Zook, H.A., Baguhl, M., Balogh, A., Bame, S.J., Fechtig, H., Forsyth, R., Hanner, M.S., Horányi, M., Kissel, J., Lindblad, B.A., Linkert, D., Linkert, G., Mann, I., McDonnell, J.A.M., Morfill, G.E., Phillips, J.L., Polanskey, C., Schwehm, G.H., Siddique, N., Staubach, P., Svestka, J., Taylor, A., 1993. Discovery of Jovian dust streams and interstellar grains by the Ulysses spacecraft. *Nature* 362, 428–430.

Hamilton, D.P., 1996. The asymmetric time-variable rings of mars. *Icarus* 119, 153–172.

Horányi, M., Szalay, J.R., Kempf, S., Schmidt, J., Grün, E., Srama, R., Sternovsky, Z., 2015. A permanent, asymmetric dust cloud around the Moon. *Nature* 522, 324–326. doi:10.1038/nature14479.

Igenbergs, E., Hüdolph, A., Uesugi, K., Hayashi, T., Svedhem, H., Iglseder, H., Koller, G., Glasmachers, A., Grun, E., Schwehm, G., Mizutani, H., Yamamoto, T., Fugimura, A., Ishii, N., Araki, H., Yamakoshi, K., Nogami, K., 1991. The Present Status of the Munich Dust Counter Experiment on Board of the HITEN Spacecraft (invited Contribution), in: Levasseur-Regoud, A.C., Hasegawa, H. (Eds.), IAU Colloq. 126: Origin and Evolution of Interplanetary Dust, p. 15. doi:10.1007/978-94-011-3640-2\_3.

Igenbergs, E., Sasaki, S., Farber, G., Fisher, F., Munzenmayer, R., Fujiwara, A., Iglseder, H., Glasmachers, A., Grun, E., Mukai, T., Nogami, K.I., Ohashi, H., Schwehm, G., Svedhem, H., Yamakoshi, K., 1996. Mars Dust Counter on Board Isas Planet-B, in: Gustafson, B.A.S., Hanner, M.S. (Eds.), IAU Colloq. 150: Physics, Chemistry, and Dynamics of Interplanetary Dust, p. 233.

Igenbergs, E., Sasaki, S., Münzenmayer, R., Ohashi, H., Färber, G., Fischer, F., Fujiwara, A., Glasmachers, A., Grün, E., Hamabe, Y., Iglseder, H., Klinge, D., Maiyamoto, H., Mukai, T., Naumann, W., Nogami, K.I., Schwehm, G.H., Svedhem, H., Yamakoshi, K., 1998. Mars dust counter. *Earth Planets Space* 50, 241–245.

Iglseder, H., Münzenmayer, R., Svedhem, H., Grün, E., 1993. Cosmic dust and space debris measurements with the Munich dust counter on board the satellites hiten and brem-sat. *Advances in Space Research* 13, 129–132. doi:10.1016/0273-1177(93)90579-Z.

Ishimoto, H., Kimura, H., Nakagawa, N., Mukai, T., 1997. Planned observation of phobos/deimos dust rings by PLANET-B. *Advances in Space Research* 19, 123–126. doi:10.1016/S0273-1177(96)00126-3.

Kawaguchi, J., Yamakawa, H., Uesugi, T., Matsuo, H., 1995. On making use of lunar and solar gravity assists in LUNAR-A, PLANET-B missions. *Acta Astronautica* 35, 633–642. doi:10.1016/0094-5765(95)00013-P.

Kimura, H., 2015. Interstellar dust in the Local Cloud surrounding the Sun. *Monthly Notices of the Royal Astro. Soc.* 449, 2250–2258. doi:10.1093/mnras/stv427.

Kobayashi, M., Krüger, H., Senshu, H., Wada, K., Okudaira, O., Sasaki, S., Kimura, H., 2018. In situ observation of dust particles of Martian dust belts by a large-sensitive-area dust sensor. *Planetary and Space Science* 156, 41–46. doi:10.1016/j.pss.2017.12.011.

Krivov, A.V., Feofilov, A.G., Dikarev, V.V., 2006. Search for the putative dust belts of Mars: The late 2007 opportunity. *Planetary and Space Science* 54, 871–878. doi:10.1016/j.pss.2006.05.007.

Krivov, A.V., Hamilton, D.P., 1997. Martian dust belts: Waiting for discovery. *Icarus* 128, 335–353.

Krüger, H., Dikarev, V., Anweiler, B., Dermott, S.F., Graps, A.L., Grün, E., Gustafson, B.A., Hamilton, D.P., Hanner, M.M.S., Horányi, M., Kissel, J., Linkert, D., Linkert, G., Mann, I., McDonnell, J.A.M., Morfill, G.E., Polanskey, C., Schwehm, G.H., Srama, R., 2010. Three years of Ulysses dust data: 2005 to 2007. *Planetary and Space Science* 58, 951–964.

Krüger, H., Kobayashi, M., Strub, P., Klostermeyer, G.M., Sommer, M., Kimura, H., Grün, E., Srama, R., 2021. Modelling cometary meteoroid stream traverses of the Martian Moons eXploration (MMX) spacecraft en route to Phobos. *Earth Planets and Space* 73, 93. doi:10.1186/s40623-021-01412-5.

Krüger, H., Strub, P., Altobelli, N., Sterken, V., Srama, R., Grün, E., 2019. Interstellar dust in the solar system: model versus in-situ spacecraft data. *Astronomy and Astrophysics* 626, A37. doi:doi.org/10.1051/0004-6361/201834316.

Krüger, H., Strub, P., Grün, E., 2024. Ulysses spacecraft in situ detections of cometary dust trails. *Philosophical Transactions of the Royal Society A* 382, 20230200. doi:10.1098/rsta.2023.0200.

Krüger, H., Strub, P., Sterken, V.J., Grün, E., 2015. Sixteen years of ulysses interstellar dust measurements in the solar system: I. mass distribution and gas-to-dust mass ratio. *Astrophysical Journal* 812, 139. doi:doi:10.1088/0004-637X/812/2/139.

Kuramoto, K., Kawakatsu, Y., Fujimoto, M., Araya, A., Barucci, M.A., Genda, H., Hirata, N., Ikeda, H., Imamura, T., Helbert, J., Kameda, S., Kobayashi, M., Kusano, H., Lawrence, D.J., Matsumoto,

K., Michel, P., Miyamoto, H., Morota, T., Nakagawa, H., Nakamura, T., Ogawa, K., Otake, H., Ozaki, M., Russell, S., Sasaki, S., Sawada, H., Senshu, H., Tachibana, S., Terada, N., Ulamec, S., Usui, T., Wada, K., Watanabe, S.i., Yokota, S., 2022. Martian moons exploration MMX: sample return mission to Phobos elucidating formation processes of habitable planets. *Earth, Planets and Space* 74, 12. doi:10.1186/s40623-021-01545-7.

Liu, X., Schmidt, J., 2021. Configuration of the Martian dust rings: shapes, densities, and size distributions from direct integrations of particle trajectories. *Monthly Notices of the Royal Astro. Soc.* 500, 2979–2985. doi:10.1093/mnras/staa3084, [arXiv:2201.02847](https://arxiv.org/abs/2201.02847).

Makuch, M., Krivov, A.V., Spahn, F., 2005. Long-term dynamical evolution of dusty ejecta from Deimos. *Planetary and Space Science* 53, 357–369. doi:10.1016/j.pss.2004.09.063.

Mann, I., 2010. Interstellar Dust in the Solar System. *Annual Review of Astronomy and Astrophysics* 48, 173–203. doi:10.1146/annurev-astro-081309-130846.

May, B.H., 2007. A survey of radial velocities in the zodiacal dust cloud. Ph.D. thesis. PhD thesis, Imperial College of Science, Technology and Medicine London, U. K.

Münzenmayer, R., Igenbergs, E., Iglseder, H., Svedhem, H., 1997. The munich dust counter on board the muses-a mission: calibration of impacts inside and in front of the detector. *Advances in Space Research* 20, 1485–1488. doi:10.1016/S0273-1177(97)00422-5.

Nakatani, I., Tsuruda, K., Yamamoto, T., 1995. Planet-B: Mars mission with small spacecraft but potentially with large science reward. *Acta Astronautica* 35, 337–344.

Naumann, W., 2000. Rechnergestützte Automatisierung eines Experiments im interplanetaren Raum. Ph.D. thesis. Technische Universität München.

Ozaki, N., Yamamoto, T., Gonzalez-Franquesa, F., Gutierrez-Ramon, R., Pushparaj, N., Chikazawa, T., Tos, D.A.D., Çelik, O., Marmo, N., Kawakatsu, Y., Arai, T., Nishiyama, K., Takashima, T., 2022. Mission design of DESTINY+: Toward active asteroid (3200) Phaethon and multiple small bodies. *Acta Astronautica* 196, 42–56. doi:10.1016/j.actaastro.2022.03.029, [arXiv:2201.01933](https://arxiv.org/abs/2201.01933).

Sasaki, S., 1999. Dust ring/torus around Mars, waiting for detection by NOZOMI. *Advances in Space Research* 23, 1907–1910. doi:10.1016/S0273-1177(99)00278-1.

Sasaki, S., Igenbergs, E., Ohashi, H., Münzenmayer, R., Naumann, W., Hofschuster, G., Born, M., Färber, G., Fischer, F., Fujiwara, A., Glasmachers, A., Grün, E., Hamabe, Y., Iglseder, H., Kawamura, T., Miyamoto, H., Morishige, K., Mukai, T., Naoi, T., Nogami, K., Schwehm, G., Svedhem, H., 2002a.

Observation of interplanetary and interstellar dust particles by Mars Dust Counter (MDC) on board NOZOMI. *Advances in Space Research* 29, 1145–1153.

Sasaki, S., Igenbergs, E., Ohashi, H., Müenzenmayer, R., Naumann, W., Born, M., Farber, G., Fisher, F., Fujiwara, A., Glasmachers, A., Gruen, E., Hamabe, Y., Hofschröter, G., Iglseder, H., Miyamoto, H., Morishige, K., Mukai, T., Nogami, K., Schwehm, G., Svedhem, H., Yamakoshi, K., 1999. Initial Results of Mars Dust Counter (MDC) on Board NOZOMI: Leonids Encounter, in: *Lunar and Planetary Science Conference*, p. 1581.

Sasaki, S., Igenbergs, E., Ohashi, H., Senger, R., Hofschröter, G., Müenzenmayer, R., Naumann, W., Grün, E., Fujiwara, A., Hamabe, Y., Mann, I., Miyamoto, H., Mukai, T., Nogami, K., Shoji, S., Svedhem, H., 2002b. Interplanetary and interstellar dust observations by Mars dust counter on board NOZOMI: four-year operation, in: Warmbein, B. (Ed.), *Asteroids, Comets, and Meteors: ACM 2002*, pp. 79–82.

Sasaki, S., Igenbergs, E., Ohashi, H., Senger, R., Müenzenmayer, R., Naumann, W., Grün, E., Nogami, K., Mann, I., Svedhem, H., 2007. Summary of interplanetary and interstellar dust observation by Mars Dust Counter on board NOZOMI. *Advances in Space Research* 39, 485–488. doi:10.1016/j.asr.2006.11.006.

Senger, R., 2007. Data handling and evaluation for autonomous experiments in interplanetary missions. Ph.D. thesis. Munich University of Technology, Germany, <https://mediatum.ub.tum.de/node?id=625799>.

Showalter, M.R., 2017. Dust at the Martian moons and in the circummartian space. The Dust, Atmospheres and Plasma Environment of the Moon and Small Bodies (DAP-2017) Workshop , [https://impact.colorado.edu/dap/2017/abstracts/mark\\_showalter.pdf](https://impact.colorado.edu/dap/2017/abstracts/mark_showalter.pdf).

Showalter, M.R., Hamilton, D.P., Nicholson, P.D., 2006. A deep search for Martian dust rings and inner moons using the Hubble Space Telescope. *Planetary and Space Science* 54, 844–854. doi:10.1016/j.pss.2006.05.009.

Simolka, J., Blanco, R., Ingerl, S., Krüger, H., Sommer, M., Srama, R., Strack, H., Wagner, C., Arai, T., Bauer, M., Fröhlich, P., Gläser, J., Gräßlin, M., Henselowsky, C., Hillier, J., Hirai, T., Ito, M., Kempf, S., Khawaja, N., Kimura, H., Klinkner, S., Kobayashi, M., Lengowski, M., Li, Y., Mocker, A., Moragas-Klostermeyer, G., Postberg, F., Rieth, F., Sasaki, S., Schmidt, J., Sterken, V.J., Sternovsky, Z., Strub, P., Trieloff, M., Szalay, J., Yabuta, H., 2024. The DESTINY+ Dust Analyser - A Dust Telescope for Analysing Cosmic Dust Dynamics and Composition. *Philosophical Transactions of the*

Royal Society A , 382:20230199doi:doi.org/10.1098/rsta.2023.0199.

Smith, S.M., Wilson, J.K., Baumgardner, J., Mendillo, M., 1999. Discovery of the distant lunar sodium tail and its enhancement following the Leonid Meteor Shower of 1998. *Geophysical Research Letters* 26, 1649–1652. doi:10.1029/1999GL900314.

Soja, R.H., Sommer, M., Herzog, J., Agarwal, J., Rodmann, J., Srama, R., Vaubaillon, J., Strub, P., Hornig, A., Bausch, L., Grün, E., 2015. Characteristics of the dust trail of 67P/Churyumov-Gerasimenko: an application of the IMEX model. *Astronomy and Astrophysics* 583, A18. doi:10.1051/0004-6361/201526184.

Soter, S., 1971. The dust belts of Mars. Technical Report. Center for Radiophysics and Space Research Report No. 462.

Srama, R., Ahrens, T. J. Altobelli, N., Auer, S., Bradley, J. G. Burton, M., Dikarev, V.V., Economou, T., Fechtig, H., Görlich, M., Grande, M., Graps, A.L., Grün, E., Havnes, O., Helfert, S., Horányi, M., Igenbergs, E., Jeßberger, E.K., Johnson, T.V., Kempf, S., Krivov, A.V., Krüger, H., Moragas-Klostermeyer, G., Lamy, P., Landgraf, M., Linkert, D., Linkert, G., Lura, F., Mocker-Ahreep, A., McDonnell, J.A.M., Möhlmann, D., Morfill, G.E., Müller, M., Roy, M., Schäfer, G., Schlotzhauer, G.H., Schwehm, G.H., Spahn, F., Stübig, M., Svestka, J., Tschernjawska, V., Tuzzolino, A.J., Wäsch, R., Zook, H.A., 2004. The Cassini Cosmic Dust Analyzer. *Space Science Reviews* 114, 465–518.

Srama, R., Kempf, S., Moragas-Klostermeyer, G., Altobelli, N., Auer, S., Beckmann, U., Bugiel, S., Burton, M., Economou, T., Fechtig, H., Fiege, K., Green, S.F., Grande, M., Havnes, O., Hillier, J.K., Helfert, S., Horanyi, M., Hsu, S., Igenbergs, E., Jessberger, E.K., Johnson, T.V., Khalisi, E., Krüger, H., Matt, G., Mocker, A., Lamy, P., Linkert, G., Lura, F., Möhlmann, D., Morfill, G., Otto, K., Postberg, F., Roy, M., Schmidt, J., Schwehm, G.H., Spahn, F., Sterken, V., Svestka, J., Tschernjawska, V., Grün, E., Röser, H.P., 2011. The Cosmic Dust Analyser onboard CASSINI: Ten years of discoveries. *CEAS Space Journal* 2, 3–16. doi:10.1007/s12567-011-0014-x.

Srama, R., Kempf, S., Moragas-Klostermeyer, G., Helfert, S., Ahrens, T.J., Altobelli, N., Auer, S., Beckmann, U., Bradley, J.G., Burton, M., Dikarev, V.V., Economou, T., Fechtig, H., Green, S.F., Grande, M., Havnes, O., Hillier, J.K., Horanyi, M., Igenbergs, E., Jessberger, E.K., Johnson, T.V., Krüger, H., Matt, G., McBride, N., Mocker, A., Lamy, P., Linkert, D., Linkert, G., Lura, F., McDonnell, J.A.M., Möhlmann, D., Morfill, G.E., Postberg, F., Roy, M., Schwehm, G.H., Spahn, F., Svestka, J., Tschernjawska, V., Tuzzolino, A.J., Wäsch, R., Grün, E., 2006. In situ dust measurements in the inner

Saturnian system. *Planetary and Space Science* 54, 967–987. doi:10.1016/j.pss.2006.05.021.

Strub, P., Krüger, H., Sterken, V.J., 2015. Sixteen years of Ulysses interstellar dust measurements in the Solar System: II. Fluctuations in the dust flow from the data. *Astrophysical Journal* 812, 140. doi:doi:10.1088/0004-637X/812/2/140.

Svedhem, H., Münzenmeyer, R., Iglseder, H., 1996. Detection of possible interstellar particles by the Hiten spacecraft, in: Gustafson, B.A.S., Hanner, M.S. (Eds.), IAU Colloq. 150: Physics, Chemistry, and Dynamics of Interplanetary Dust, pp. 27–30.

Swaczyna, P., Bzowski, M., Heerikhuisen, J., Kubiak, M.A., Rahmanifard, F., Zirnstein, E.J., Fuselier, S.A., Galli, A., McComas, D.J., Möbius, E., Schwadron, N.A., 2023. Interstellar Conditions Deduced from Interstellar Neutral Helium Observed by IBEX and Global Heliosphere Modeling. *Astrophysical Journal* 953, 107. doi:10.3847/1538-4357/ace719, arXiv:2307.06694.

Szalay, J.R., Poppe, A.R., Agarwal, J., Britt, D., Belskaya, I., Horányi, M., Nakamura, T., Sachse, M., Spahn, F., 2018. Dust Phenomena Relating to Airless Bodies. *Space Science Reviews* 214, 98. doi:10.1007/s11214-018-0527-0.

Westphal, A.J., Achilles, C., Allen, C., Ansari, A., Bajt, S., Bassim, N., Bastien, R., Bechtel, H.A., Borg, J., Brenker, F.E., Bridges, J., Brownlee, D.E., Burchell, M., Burghammer, M., Butterworth, A., Changela, H., Cloetens, P., Davis, A.M., Floss, C., Flynn, G., Fougeray, P., Frank, D., Gainsforth, Z., Gruen, E., Heck, P.R., Hillier, J.K., Hoppe, P., Hudson, B., Huss, G.R., Huth, J., Hvide, B., Kearsley, A., King, A.J., Lai, B., Leitner, J., Lemelle, L., Leonard, A., Leroux, H., Lettieri, R., Marchant, W., Nittler, L.R., Ogliore, R., Postberg, F., Price, M.C., Sandford, S.A., Sans Tresseras, J.A., Schmitz, S., Schoonjans, T., Schreiber, K., Silversmit, G., Simionovici, A., Sole, V.A., Srama, R., Stephan, T., Sterken, V., Stodolna, J., Stroud, R.M., Sutton, S., Treiloff, M., Tsou, P., Tsuchiyama, A., Tyliszczak, T., Vekemans, B., Vincze, L., Wordsworth, N., Zevin, D., Zolensky, M.E., > 30,000 Stardust@Home Dusters, 2012. Status of the Stardust ISPE and the Origin of Four Interstellar Dust Candidates, in: *Lunar and Planetary Institute Science Conference Abstracts*, p. 2084.

Witte, M., 2004. Kinetic parameters of interstellar neutral helium. Review of results obtained during one solar cycle with the Ulysses/GAS-instrument. *Astronomy and Astrophysics* 426, 835–844. doi:10.1051/0004-6361:20035956.

Yamamoto, T., Tsuruda, K., 1998. The PLANET-B mission. *Earth, Planets and Space* 50, 175–181. doi:10.1186/BF03352100.

Yang, K., Schmidt, J., Feng, W., Liu, X., 2022. Distribution of dust ejected from the lunar surface into the Earth-Moon system. *Astronomy and Astrophysics* 659, A120. doi:10.1051/0004-6361/202140810, [arXiv:2204.01040](https://arxiv.org/abs/2204.01040).

Yoshikawa, M., Kawaguchi, J., Yamakawa, H., Kato, T., Ichikawa, T., Ohnishi, T., Ishibashi, S., 2005. Summary of the orbit determination of NOZOMI spacecraft for all the mission period. *Acta Astronautica* 57, 510–519. doi:10.1016/j.actaastro.2005.03.053.

Zakharov, A., Horanyi, M., Lee, P., Witasse, O., Cipriani, F., 2014. Dust at the Martian moons and in the circummartian space. *Planetary and Space Science* 102, 171–175. doi:10.1016/j.pss.2013.12.011.

Table 1 : Nozomi MDC data. Col. (1): Impact Number, (2) Impact identifier, (3) and (4): Impact day and time (UTC), (5): Particle mass (kg), (6): Particle impact speed ( $\text{km s}^{-1}$ ), (7): Impact position on dust sensor (EC: electron channel, EC.COL: electron collector, IC: ion channel, IC.COL: ion collector, GRID. EC: entrance grid, MLI.A/B: MLI outside sensor box), (8): Spacecraft spin angle during dust particle impact ( $^\circ$  at 0° MDC points closest to the Sun direction, i.e. close to the ecliptic plane), (9): Quality parameter of dust impact measurement, (10) to (12): Spacecraft position vector in heliocentric coordinate system (km), (13): Heliocentric spacecraft distance during dust impact (AU), (14) to (16): heliocentric dust particle velocity vector (km/s), (17): heliocentric speed of dust particle ( $\text{km s}^{-1}$ ), (18) and (19): Inclination and eccentricity of dust particle trajectory. See text for details.

Num.	Imp. ID	Date	Time	Mass	Speed	ImpPos	Spinph	Qua	PosX	PosY	PosZ	Rad	AbsvX	AbsvY	AbsvZ	Incl	Ecc	
(1)	(2)	(3)	(4)	(5)	(6)	(7)	(8)	(9)	(10)	(11)	(12)	(13)	(14)	(15)	(16)	(17)	(18)	(19)
1	98071101-26	10-Jul-1998	15:08:21	3.0E-15	31.57	IC.COL	331.04	189	47071711	-144794138	28784	1.02	1.32	5.19	16.83	17.66	80.36	0.67
2	98071601-3	16-Jul-1998	03:32:01	4.4E-12	15.24	EC	107.53	165	60278018	-139746168	63454	1.02	42.13	9.46	2.77	43.27	3.73	1.14
3	98073001-5	28-Jul-1998	23:23:54	1.0E-10	7.69	EC.COL	211.03	174	88381925	-123617666	59061	1.02	26.34	10.01	0.60	28.18	1.26	0.27
4	98073101-29	31-Jul-1998	06:37:46	1.3E-13	34.14	IC	270.13	180	93191670	-119958656	49421	1.02	17.86	-8.56	18.23	26.92	64.09	0.67
5	98080701-3	5-Aug-1998	11:14:40	1.7E-14	20.04	IC.COL	335.83	188	102884667	-111488040	27355	1.01	23.22	25.17	-19.06	39.19	29.48	0.76
6	98082201-8	22-Aug-1998	00:48:36	1.6E-14	25.34	EC	23.55	154	129049547	-78765918	55978	1.01	16.05	25.81	25.42	39.62	39.91	0.79
7	98090501-14	2-Sep-1998	21:28:35	6.7E-13	9.89	EC.COL	56.12	196	141712211	-51326819	44935	1.01	12.42	30.13	9.35	33.91	16.03	0.31
8	98092201-9	21-Sep-1998	10:30:04	1.4E-15	37.41	IC	139.35	125	149955432	-4648768	-13933	1.00	31.36	17.20	15.68	39.05	40.81	0.91
9	98092201-23	22-Sep-1998	00:23:40	1.6E-15	35.85	IC	321.15	149	149929104	-3207880	-4758	1.00	-0.64	0.30	-21.42	21.43	89.22	0.48
10	98101401-21	13-Oct-1998	03:45:06	2.1E-15	36.46	IC.C	304.89	189	140661832	48872548	470810	1.00	-11.78	41.10	-33.67	54.42	38.27	2.32
11	98102701-37	26-Oct-1998	10:07:48	8.5E-15	28.64	IC.COL	302.12	161	125317767	79079706	597923	0.99	-18.69	30.97	-27.82	45.63	37.57	1.32
12	98110901-29	8-Nov-1998	11:38:43	1.3E-13	16.82	IC.C	4.92	179	103639158	104886737	624512	0.99	-27.04	22.46	-15.91	38.58	24.41	0.66
13	98110901-17	8-Nov-1998	23:02:03	1.9E-13	17.15	MLI.A	342.11	148	102744228	105734878	623866	0.99	-29.88	25.74	-14.29	41.95	19.94	0.96
14	98111001-1	9-Nov-1998	10:35:00	N/A	N/A	GRID. EC	331.88	153	101823105	106580827	623077	0.99	N/A	N/A	N/A	N/A	N/A	N/A
15	98111701-8	17-Nov-1998	04:23:19	1.5E-11	11.86	EC.C	164.93	176	86086726	119183754	591866	0.98	-16.68	25.48	-1.92	30.51	3.95	0.36
16	98111801-1	17-Nov-1998	17:02:59	6.0E-11	13.92	IC.COL	75.37	184	84951085	11996169	588452	0.98	-16.51	16.49	-11.15	25.86	25.90	0.30
17	98111801-6	18-Nov-1998	00:35:19	3.3E-13	26.09	EC.C	154.95	197	84273081	120428155	586334	0.98	-5.42	33.13	-5.33	33.99	13.04	0.73
18	98112101-6	20-Nov-1998	10:39:41	1.9E-11	10.80	EC.C	305.90	208	78952092	123855597	568035	0.98	-31.47	21.21	-7.59	38.70	11.32	0.66
19	98120201-17	1-Dec-1998	18:58:50	1.5E-13	17.46	MLI.A	25.05	144	52213696	13691326	431437	0.98	-23.47	8.47	-16.74	30.04	33.86	0.02
20	98120301-9	2-Dec-1998	18:41:39	1.6E-16	50.90	IC.C	329.59	151	49768815	137804201	415244	0.98	-44.21	15.97	-48.35	67.43	45.80	4.02
21	98121801-35	17-Dec-1998	10:17:34	2.0E-12	19.65	IC.COL	335.96	214	12054841	146232969	65009	0.98	-30.29	1.67	-19.97	36.32	33.37	0.46
22	99011201-43	11-Jan-1999	17:36:43	4.6E-12	8.89	MLI.B	213.79	153	-60090702	133262786	3301958	0.98	-25.75	-19.00	5.91	32.54	11.03	0.26
23	99030104-29	1-Mar-1999	09:40:43	1.6E-16	69.58	IC.C	343.43	193	-152913439	40468814	7845675	1.06	-68.94	4.25	24.34	73.23	57.20	2.07
24	99030901-3	5-Mar-1999	22:01:49	4.1E-16	47.41	IC	122.56	159	-157266556	29378881	8067958	1.07	31.34	-11.02	14.82	36.37	72.88	0.93
25	99030901-31	8-Mar-1999	19:07:38	6.8E-12	7.95	MLI.A	335.04	85	-159641635	22221957	8188819	1.08	-7.80	-24.77	-6.26	26.71	14.46	0.20

Table 2. : Nozomi MDC data. Table 1 continued.

Num.	Imp. ID	Date	Time	Mass	Speed	ImpPos	Spinph	Qua	PosX	PosY	PosZ	Rad	AbsVX	AbsvY	AbsvZ	Incl	Ecc	
(1)	(2)	(3)	(4)	(5)	(6)	(7)	(8)	(9)	(10)	(11)	(12)	(13)	(14)	(15)	(16)	(17)	(18)	(19)
26	99042001-29	20-Apr-1999	09:14:18	3.3E-13	10.18	EC_COL	197.18	151	-160847494	-81802403	8235059	1.21	15.15	-20.76	3.25	25.91	8.13	0.17
27	99052701-39	27-May-1999	00:50:57	1.5E-13	16.78	EC	65.13	135	-121929404	-163506611	6228099	1.31	27.58	-20.13	-13.39	36.68	21.43	0.99
28	99060201-15	1-Jun-1999	18:55:49	2.1E-11	4.23	MLI_B	143.57	150	-113496558	-162463142	5794150	1.33	19.41	-14.17	-2.78	24.19	6.83	0.13
29	99071201-29	11-Jul-1999	08:00:29	1.3E-12	12.45	EC_COL	233.57	152	-45209701	-205043548	2284434	1.40	26.48	1.79	5.83	27.18	13.09	0.32
30	99072401-34	21-Jul-1999	16:10:04	4.2E-11	6.38	EC	78.79	151	-25529578	-210589673	1273877	1.42	26.26	-2.93	-5.64	27.02	12.05	0.17
31	99091201-12	11-Sep-1999	13:53:33	2.1E-14	18.55	EC_COL	11.78	122	73154780	-203522168	-3790628	1.45	37.73	14.96	-3.48	40.74	5.03	1.70
32	99092401-7	15-Sep-1999	03:27:15	1.4E-10	6.76	EC_COL	242.93	172	7962563	-200929557	-4124835	1.45	20.13	13.83	3.32	24.65	7.77	0.22
33	99101901-45	18-Oct-1999	09:37:27	3.8E-15	44.83	MLI_B	118.35	194	132995420	-165734631	-6863033	1.42	1.00	48.32	-27.55	55.63	42.84	3.08
34	99112001-13	20-Nov-1999	03:51:16	2.3E-09	3.04	EC_COL	72.77	131	170868118	-112651281	-8803966	1.37	9.71	23.82	-2.49	25.84	6.59	0.19
35	99112501-3	24-Nov-1999	23:36:37	3.6E-12	26.72	IC_COL	193.32	222	174817334	-103541015	-9005852	1.36	-15.37	31.53	5.02	35.43	11.19	0.98
36	00040501-19	2-Apr-2000	15:23:17	1.9E-13	17.18	MLI_A	357.98	143	50731385	142029583	-2592619	1.01	-48.18	8.82	1.96	49.02	2.38	1.72
37	00041101-7	5-Apr-2000	16:51:25	N/A	N/A	GRID-EC	206.63	107	42452439	14386305	-2166598	1.00	N/A	N/A	N/A	N/A	N/A	N/A
38	00041601-8	12-Apr-2000	01:28:10	4.5E-15	34.44	IC	167.12	160	24907116	146475307	-1264008	0.99	-29.54	-31.05	-3.49	42.99	9.02	1.02
39	00052301-36	17-May-2000	07:38:15	5.1E-14	23.97	IC	58.23	155	-71787710	127846302	3706283	0.98	-39.43	-31.41	-12.65	51.97	14.11	1.97
40	00052301-29	20-May-2000	04:29:12	1.6E-11	5.55	IC_COL	198.85	169	-78913331	123954539	4072244	0.98	-24.52	-20.40	2.54	32.00	5.04	0.18
41	00061301-19	9-Jun-2000	20:39:49	N/A	N/A	EC_COL	176.00	183	-123356560	87376625	6534660	1.01	N/A	N/A	N/A	N/A	N/A	N/A
42	00062101-42	17-Jun-2000	07:46:12	N/A	N/A	GRID-EC	41.84	148	-135938575	71223534	6398044	1.03	N/A	N/A	N/A	N/A	N/A	N/A
43	00062101-37	19-Jun-2000	08:42:39	4.0E-12	5.07	IC_C	192.79	108	-139013539	66608656	7155521	1.03	-12.12	-27.67	1.39	30.24	3.80	0.07
44	00062101-4	19-Jun-2000	11:51:26	3.1E-13	10.88	EC_COL	223.90	151	-139206255	66309094	7165554	1.03	-7.96	-30.02	5.73	31.58	11.41	0.23
45	00070701-22	30-Jun-2000	05:52:23	5.1E-12	12.71	MLI_A	230.14	147	-152766946	40869640	7859392	1.06	-1.49	-30.94	6.98	31.75	13.84	0.28
46	00070701-26	30-Jun-2000	18:13:38	2.6E-13	8.60	EC	175.17	102	-153307441	39615177	7866932	1.06	-3.62	-28.61	-0.34	28.84	2.87	0.13
47	00070701-29	3-Jul-2000	19:07:25	4.3E-12	10.46	EC_COL	110.52	126	-156281040	32162643	8038908	1.07	-4.06	-31.92	-6.72	32.88	11.96	0.31
48	00072601-17	22-Jul-2000	12:16:06	2.8E-12	9.02	MLI_B	164.36	199	-167002683	-1488730	8884081	1.12	5.54	-26.32	-2.07	26.97	5.02	0.15
49	00081301-3	6-Aug-2000	12:18:13	2.0E-13	8.39	EC_COL	165.72	127	-166716711	-51676975	8564725	1.17	9.95	-23.56	-2.06	25.66	5.18	0.17
50	00081801-37	15-Aug-2000	18:05:25	1.7E-10	6.49	EC	168.49	174	-163003944	-73553807	8370791	1.20	11.00	-22.61	-1.57	25.19	4.40	0.15
51	00092901-3	25-Sep-2000	15:04:09	3.5E-11	16.39	EC_COL	194.85	178	-121162129	-154420890	6208188	1.31	20.83	-2.97	1.41	21.08	5.75	0.58
52	00101201-16	7-Oct-2000	17:52:39	7.3E-12	21.79	EC_COL	209.09	182	-102758167	-172353058	5259521	1.34	21.82	4.72	5.76	23.05	20.73	0.67
53	00101501-37	13-Oct-2000	14:04:38	2.3E-12	8.62	MLI_B	243.85	155	-93199460	-179901458	4766798	1.35	21.72	-7.86	4.29	23.49	10.87	0.20
54	00103001-22	24-Oct-2000	14:48:28	3.7E-12	6.81	IC_COL	153.98	146	-74153407	-192156991	3785745	1.38	20.10	-5.18	-3.36	21.03	9.19	0.33
55	00103001-13	27-Oct-2000	00:45:25	3.2E-12	5.55	EC	164.71	140	-69338166	-194489332	3563473	1.38	19.99	-5.41	-2.27	20.84	6.28	0.33
56	01012501-8	9-Jan-2001	06:44:50	2.7E-11	3.99	EC	220.25	155	70699447	-204417263	-3665361	1.45	21.30	10.61	1.42	23.84	3.45	0.15
57	01012501-19	19-Jan-2001	13:17:01	7.4E-17	62.40	IC_COL	85.03	153	88861867	-196719539	-4598394	1.44	-3.31	46.49	43.78	63.94	69.39	4.10
58	01012501-29	21-Jan-2001	19:41:04	6.5E-13	26.36	EC_COL	214.72	175	92751876	-194750035	-4788212	1.44	24.30	34.16	-11.27	43.41	17.79	1.89
59	01030701-32	2-Mar-2001	17:23:13	3.1E-15	42.48	IC_COL	250.97	163	151659347	-144638115	-7821226	1.40	-4.70	45.71	-27.42	53.51	43.93	2.80
60	01030701-42	4-Mar-2001	04:39:46	2.8E-12	11.86	EC	338.64	162	153407510	-142285263	-7910657	1.40	2.37	16.94	-4.25	17.62	18.35	0.69

Table 3. : Nozomi MDC data. Table 1 continued.

Num.	Imp. ID	Date	Time	Mass	Speed	ImpPos	Spinph	Qua	PosX	PosY	PosZ	Rad	AbsX	AbsY	AbsZ	Incl	Ecc	
(1)	(2)	(3)	(4)	(5)	(6)	(7)	(8)	(9)	(10)	(11)	(12)	(13)	(14)	(15)	(16)	(17)	(18)	
61	01034401-28	14-Mar-2001	03:56:34	1.6E-12	12.86	IC	238.27	156	164272640	-125429220	-8467062	1.38	5.26	29.21	-7.72	30.67	17.54	0.60
62	01031401-30	14-Mar-2001	04:32:27	N/A	N/A	GRID_EC	317.20	127	164297309	-125355114	-8468330	1.38	N/A	N/A	N/A	N/A	N/A	N/A
63	01042801-49	13-Apr-2001	03:21:54	N/A	N/A	GRID_EC	48.74	161	185210475	-66819656	-9566246	1.32	N/A	N/A	N/A	N/A	N/A	N/A
64	01042801-43	25-Apr-2001	18:20:58	N/A	N/A	GRID_EC	47.68	154	187835574	-39757497	-9667764	1.29	N/A	N/A	N/A	N/A	N/A	N/A
65	01051701-6	12-May-2001	03:53:34	2.3E-13	40.38	EC	24.35	131	185013498	-3160239	-9517613	1.24	-20.86	-8.85	12.60	25.93	128.56	0.82
66	01070201-6	11-Jun-2001	06:08:30	6.0E-11	7.93	EC_C	307.05	161	159342208	63034534	-8188556	1.15	-16.68	17.61	-3.57	24.52	10.43	0.42
67	01070201-50	21-Jun-2001	12:59:31	N/A	N/A	EC	348.35	107	144147630	83721769	-7404466	1.12	N/A	N/A	N/A	N/A	N/A	N/A
68	01070201-40	22-Jun-2001	08:06:52	N/A	N/A	GRID_EC	350.95	148	142835570	85253451	-7336773	1.11	N/A	N/A	N/A	N/A	N/A	N/A
69	01070201-1	29-Jun-2001	09:35:55	7.0E-12	10.29	EC_C	72.20	200	130348109	98285898	-6692756	1.09	-22.57	13.19	8.33	27.44	18.30	0.39
70	01071101-3	2-Jul-2001	05:38:10	6.2E-12	8.72	MLI_A	315.84	140	124917369	103219225	-6412911	1.08	-21.18	12.28	-3.16	24.69	8.93	0.42
71	01071101-14	3-Jul-2001	08:32:53	N/A	N/A	MLI_A	5.27	123	122701224	105114802	-6298786	1.08	N/A	N/A	N/A	N/A	N/A	N/A
72	01080701-35	6-Aug-2001	13:30:43	N/A	N/A	IC_C	338.07	162	40249764	144297129	-2053286	1.00	N/A	N/A	N/A	N/A	N/A	N/A
73	01081601-39	11-Aug-2001	06:49:33	4.7E-12	8.59	MLI_A	335.70	145	27219203	14622479	-1382973	0.99	-25.03	-0.60	-0.88	25.05	2.22	0.36
74	01081601-8	14-Aug-2001	17:12:07	7.1E-13	16.72	EC_COL	249.57	165	17568823	147008013	-886524	0.99	-31.95	-10.70	-9.37	34.97	17.25	0.53
75	01081601-14	14-Aug-2001	23:33:07	1.6E-15	33.47	EC_COL	254.80	187	16885348	147047013	-851363	0.99	-29.44	-22.47	-21.12	42.63	38.56	1.02
76	01091201-33	31-Aug-2001	01:13:26	2.2E-12	13.66	EC	272.86	163	-28290410	143408893	1471372	0.98	-25.41	-14.07	-7.99	30.13	15.94	0.30
77	01091201-24	8-Sep-2001	22:14:27	6.4E-11	5.40	EC	336.09	161	-52485293	136371100	2714743	0.98	-25.69	-11.09	0.19	27.98	1.15	0.14
78	01091201-35	10-Sep-2001	04:43:43	N/A	N/A	GRID_EC	251.15	113	-55854359	135073123	2887877	0.98	N/A	N/A	N/A	N/A	N/A	N/A
79	01101501-15	7-Oct-2001	06:07:38	1.1E-12	28.96	IC	297.95	207	-118445072	92784313	6100899	1.01	0.11	-17.25	-16.57	23.92	50.08	0.57
80	01101501-37	8-Oct-2001	20:27:08	1.7E-13	13.84	MLI_A	338.82	108	-1214445047	89542857	6254968	1.01	-10.17	-16.33	-1.93	19.33	6.05	0.58
81	01102601-47	25-Oct-2001	20:22:45	1.2E-13	14.26	EC_COL	105.12	165	-147692924	51559764	7599835	1.05	-3.70	-29.54	9.99	31.40	19.65	0.24
82	01110301-43	29-Oct-2001	16:13:37	9.2E-12	8.45	MLI_A	302.39	113	-152106974	42349726	7825425	1.06	-7.44	-23.83	-4.51	25.37	10.70	0.23
83	01110301-50	30-Oct-2001	06:59:05	6.5E-15	34.04	IC_C	336.93	144	-152762671	40854760	785899	1.06	7.91	-1.62	-9.16	12.20	9.3.10	0.91
84	01110301-8	1-Nov-2001	18:22:40	N/A	N/A	GRID_EC	335.30	112	-155260426	34800106	7986757	1.06	N/A	N/A	N/A	N/A	N/A	N/A
85	01112101-3	16-Nov-2001	12:16:52	N/A	N/A	GRID_EC	263.72	93	-165364919	-2030892	8501495	1.11	N/A	N/A	N/A	N/A	N/A	N/A
86	01120901-40	2-Dec-2001	22:06:35	N/A	N/A	GRID_EC	346.16	143	-167460239	-42873428	8603767	1.16	N/A	N/A	N/A	N/A	N/A	N/A
87	01121801-31	15-Dec-2001	17:18:10	6.0E-13	27.87	EC_C	37.13	173	-163047897	-73317671	8373146	1.20	7.11	-1.35	11.18	13.32	70.08	0.81
88	02020501-2	26-Jan-2002	20:50:42	6.4E-13	14.15	MLI_B	339.83	123	-119420615	-156340981	6118480	1.32	8.61	-7.41	-4.43	12.20	21.46	0.78
89	02020501-30	1-Feb-2002	04:10:21	1.9E-13	14.51	MLI_B	33.71	152	-115254003	-164433827	5711383	1.33	9.78	-6.04	4.54	12.35	21.68	0.77
90	02021501-31	10-Feb-2002	19:09:15	2.2E-12	29.10	EC	320.80	180	-9622343	-177633575	4922522	1.35	1.55	4.60	-13.95	14.77	9.3.42	0.72
91	02021501-14	12-Feb-2002	00:27:34	1.6E-13	15.72	EC	247.28	147	-9420049	-179153738	4818354	1.35	22.52	-3.10	-11.50	25.47	27.92	0.31
92	02023501-25	23-Feb-2002	05:15:40	7.4E-13	31.35	EC_C	288.19	178	-74176778	-19177021	3425042	1.38	8.84	8.41	-22.29	25.41	76.82	0.45
93	02032301-8	19-Mar-2002	17:27:36	N/A	N/A	EC_COL	337.50	104	-29441565	-209681925	1483894	1.42	N/A	N/A	N/A	N/A	N/A	N/A
94	02032301-12	22-Mar-2002	20:37:50	N/A	N/A	GRID_EC	16.17	145	-23430977	-211023843	1174685	1.42	N/A	N/A	N/A	N/A	N/A	N/A
95	02033101-7	27-Mar-2002	05:49:45	9.5E-13	9.11	IC_C	331.52	153	-14980509	-21250436	739853	1.42	14.11	-1.18	-4.31	14.80	16.92	0.65
96	02041401-34	1-Apr-2002	13:17:15	8.4E-13	12.84	EC	308.41	119	-4703522	-213835193	211179	1.43	12.48	1.60	-8.34	15.10	33.82	0.64